Diploma thesis

Trajectory Modelling of Match Balloon Soundings for Cirrus Cloud Characterisation

Presented by

Ines Engel

Zurich, November 2009

University of Münster
Faculty of Geosciences
Institute of Landscape Ecology

Supervisors

Prof. Dr. Otto Klemm	University of Münster
Prof. Dr. Thomas Peter	Swiss Federal Institute of Technology Zurich

Advisor

Dr. Frank G. Wienhold	Swiss Federal Institute of Technology Zurich

Contents

Abstract vi

Zusammenfassung vii

1 Introduction 1
- 1.1 Motivation . . . 1
- 1.2 Physical background . . . 2
  - 1.2.1 Cirrus clouds . . . 2
  - 1.2.2 Balloon soundings . . . 3
- 1.3 Establishment of the match technique . . . 3

2 Material and Methods 5
- 2.1 Study sites . . . 5
- 2.2 Measurement equipment . . . 6
  - 2.2.1 Balloon sonde . . . 6
  - 2.2.2 COBALD backscatter sonde . . . 6
  - 2.2.3 Snow White hygrometer . . . 8
- 2.3 Modelling of match balloon soundings . . . 10
  - 2.3.1 Numerical weather prediction models . . . 10
  - 2.3.2 Trajectory modelling . . . 12
  - 2.3.3 Calculation of single balloon soundings . . . 13
  - 2.3.4 Calculation of match balloon soundings . . . 13

3 Results 20
- 3.1 Exemplary model results . . . 20
- 3.2 Probability of a favourable match situation . . . 27
- 3.3 Performed match sounding . . . 28
  - 3.3.1 Forecast situation . . . 28
  - 3.3.2 Analysis of the match flight . . . 31
  - 3.3.3 Measurement results . . . 36

4 Discussion and Conclusion 39

5 Outlook 42

References 44

List of Figures

2.1 Colour index as function of the particle radius. 8
2.2 Temporal domains of COSMO-2, COSMO-7, and ECMWF. 11
2.3 Spatial domains of COSMO-2, COSMO-7, and ECMWF. 11
2.4 Sketch of the model's working steps. 14
2.5 Sketch of the model's working steps – backward mode. 15
2.6 Topographic map of Switzerland. 16
2.7 Sketch of the model's match distance criterion. 17
2.8 Examplary model output in Google Earth. 19

3.1 Model result of the 22nd April 2009. 21
3.2 Model result of the 8th August 2009. 22
3.3 Model result of the 16th July 2009. 24
3.4 Model result of the 8th June 2009. 25
3.5 Model result of the 23rd June 2009. 26
3.6 Model result of the 6th July 2009. 29
3.7 Modified model result of the 6th July 2009. 30
3.8 Deviations of computed and recorded balloon tracks. 32
3.9 Balloons' climbing rates. 33
3.10 Deviations of modified computed and recorded balloon tracks. 33
3.11 Match validation: Zurich. 34
3.12 Match validation: Payerne. 34
3.13 Trajectory errors. 35
3.14 Vertical humidity and temperature profiles for Payerne and Zurich. 37
3.15 Vertical backscatter profiles for Payerne and Zurich. 38
3.16 LIDAR image. 38

List of Tables

3.1 Starting locations and times for the second balloon on 16th July 2009 . . . 24
3.2 Starting locations and times for the second balloon on 8th June 2009 . . . 25
3.3 Starting locations and times for the first balloon on 23rd June 2009 26
3.4 Frequency of favourable days for match soundings. 28
3.5 Starting locations and times for the second balloon on 6th July 2009 . . . 29
3.6 Modified starting locations and times for the second balloon on 6th July 2009. 30

List of Abbreviations

ABSR	Aerosol Backscatter Ratio
AHTD	Absolute Horizontal Transport Deviation
AN	Analysis
ATC	Air Traffic Control
BSR	Backscatter Ratio
CALIOP	Cloud-Aerosol Lidar with Orthogonal Polarization
CALIPSO	Earth-orbiting Cloud-Aerosol Lidar and Infrared Pathfinder Satellite Observations
CI	Colour Index
COBALD	Compact Optical Backscatter Aerosol Detector
COSMO	Consortium for Small-Scale Modelling
COST	European Cooperation in Science and Technology
DWD	Deutscher Wetterdienst
EASOE	European Arctic Stratospheric Ozone Experiment
ECMWF	European Centre for Medium Range Weather Forecasts
ETH	Eidgenössische Technische Hochschule; Swiss Federal Institute of Technology
FC	Forecast
GPS	Global Positioning System
IAC	Institute for Atmospheric and Climate Science
ISSR	Ice Supersaturated Regions
KML	Keyhole Markup Language
LAGRANTO	Lagrangian Analysis Tool
LED	Light Emitting Diode
LIDAR	Light Detection and Ranging
NWP	Numerical Weather Prediction
RHTD	Relative Horizontal Transport Deviation
UTC	Universal Time Coordinated

List of Symbols

D	Diameter
e	Vapour pressure
e_{ice}	Saturation vapour pressure with respect to ice
λ	Wavelength
n	Refraction index
RH	Relative humidity
RH_{ice}	Relative humidity with respect to ice
σ	Standard deviation
t	Time
T	Temperature
T_{air}	Air temperature
T_{dew}	Dew point temperature
T_{frost}	Frost point temperature
v	Wind field
X	Position vector of an air parcel

Abstract

Match balloon soundings are performed to observe evolution and life cycle of clouds with special focus on cirrus clouds. The launched equipment includes the lightweight particle backscatter sonde COBALD and the Snow White Hygrometer. Via the atmospheric backscatter signal it is possible to detect clouds and connect this information to the simultaneously measured relative humidity. The "match technique" adopts the Lagrangian perspective by coupled soundings aiming for the same air mass at different times. Within the framework of this diploma thesis a tool to coordinate two balloon soundings is developed to forecast their launching locations, times, and flight paths.
The MeteoSwiss radiosounding site at Payerne, Switzerland, is taken as the fixed starting point for one sounding. Within the greater area of Zurich the best launch position to be reached by a mobile team is determined by the new matching tool. Wind fields from the short-range forecasts of the COSMO numerical weather prediction model (run by MeteoSwiss) and the long-range ECMWF forecasts are used to calculate three-dimensional kinematic trajectories. After simulating the balloon track starting from Payerne, the trajectories of air parcels encountered during the ascent in a prescribed target region between 6 and 12 km are followed. Depending on the weather situation it is possible for forward or backward trajectories to reach the area around Zurich. The forecasting tool yields optimal launch coordinates to achieve a match for each trajectory. To estimate to what extent the given meteorological situation is in favour of a match launch near Zurich, the minimum distances of all potential second launches to all given air trajectories are evaluated on isentropic surfaces.
Results from different exemplary model runs are presented to demonstrate the spectrum of quality criteria to be fulfilled before realising a match sounding. Systematic interpretation of each day's forecast for the period from 1st April to 31st August 2009 allows assessment of the probability of suitable weather situations for match flights. About 20 % of the evaluated time could have been chosen for a match sounding with the goal of cirrus clouds characterisation. One match sounding was carried out and is analysed and discussed in detail. During the executed flights technical difficulties caused a slower climbing rate than assumed for one balloon with the result of missing its vertical target level. Nevertheless, the aim of reaching a horizontal match radius better than 10 km was achieved for the conducted match soundings after adjusting the assumed values to their real magnitude. Further practical applications will provide the feasibility of the presented forecasting tool.

Zusammenfassung

Aufeinander abgestimmte Ballonsondierungen ermöglichen es, die Entstehung und zeitliche Veränderung von Wolken zu erfassen. Die von dem Ballon getragenen Messinstrumente, eine Kombination aus der Rückstreusonde COBALD und dem Snow White Taupunktspiegel, erlauben es über die Erfassung der atmosphärischen Rückstreuung Wolken zu detektieren und diese Information mit der gemessenen Feuchte zu verknüpfen. Zwei Messungen, die zu unterschiedlichen Zeitpunkten an zwei verschiedenen Orten in derselben Luftmasse aufgenommen wurden, beschreiben ein so genanntes „Match“. Ziel des im Rahmen dieser Diplomarbeit entwickelten Vorhersagemodells ist es, die koordinierten Orte und Zeitpunkte der Ballonstarts sowie deren Flugbahnen vorherzusagen, um ein ideales Match zur Charakterisierung von Cirrus Wolken zu erzielen.
Alle Ballonsondierungen werden innerhalb der Schweiz gestartet, wobei die in Payerne gelegene Ballonsondierungsstation der MeteoSchweiz als fester Startpunkt gewählt ist. Ein mobiles Team ist jeweils im Großraum von Zürich für die Durchführung des zweiten Ballonstarts zuständig. Die zur Berechnung der Trajektorien verwendeten dreidimensionalen Windfelder resultieren von dem numerischen Wetterprognosemodell COSMO (betrieben von MeteoSchweiz) sowie dem Europäischen Zentrum für mittelfristige Wettervorhersagen. Auf der Trajektorie, die den Weg des Ballons von Payerne beschreibt, werden im Höhenbereich zwischen 6 und 12 km Luftpakete ausgewählt, deren Bewegungen weiter verfolgt werden. Das Vorhersagetool berechnet für ein Match eine Auswahl optimaler Koordinaten und Startzeiten für eine zweite Sondierung sowie Parameter, anhand derer sich die Eignung der Wettersituation bewerten lässt.
Ergebnisse verschiedener Modellläufe werden präsentiert und zeigen das Spektrum der Kriterien auf, die für einen Matchflug vorausgesetzt werden. Über die täglich analysierten Vorhersagen innerhalb des Zeitraums vom 1. April bis zum 31. August 2009 lässt sich die Wahrscheinlichkeit von geeigneten Wetterlagen für die Realisierung eines Matches abschätzen. Rund 20 % der Tage innerhalb des ausgewerteten Zeitraumes bieten entsprechende Bedingungen für Match-Sondierungen mit dem Ziel Cirrus Wolken zu charakterisieren. Eine durchgeführte Match-Sondierung wird im Rahmen dieser Arbeit detailliert betrachtet. Technische Schwierigkeiten führten dazu, dass die angestrebte Matchhöhe von einem der Ballons verfehlt wurde. Dennoch wurde das Ziel erreicht, das Luftpaket innerhalb eines horizontalen Radius kleiner 10 km ein zweites Mal anzunähern. Über nachträgliche Anpassungen der Eingangsparameter ist dieses Ergebnis vom entwickelten Programm vorhergesagt worden. Die Durchführung zukünftiger Matchflüge kann die Anwendbarkeit des Vorhersagemodells bestätigen.

1 Introduction

1.1 Motivation

Cirrus clouds are important to understand the complex mechanisms of climate change, though their radiative forcing represents still one of the largest sources of uncertainty (IPCC, 2007). Measurements of e.g. water vapour inside clouds are often representative for a single moment, but do not reveal their time evolution. Therefore, the European Cooperation in Science and Technology (COST) project "Lagrangian Measurements and Modeling of Cirrus clouds" (LAMMOC) focuses on the improvement of understanding the development and life cycle of cirrus clouds in the midlatitude regions. LAMMOC belongs to the "Atmospheric Water Vapour in the Climate System" (WaVaCS) action and started recently at the Institute for Atmospheric and Climate Science (IAC) at the Swiss Federal Institute of Technology (ETH) Zurich. The present diploma thesis is embedded into LAMMOC.

The idea of tracing cloud evolution by measurements is put into practice by using the "match technique". Two subsequent balloon soundings are coordinated with the goal of measuring the same air mass twice. In both flights, the balloons carry a payload made up of water vapour instruments and an optical backscatter sonde. Via the atmospheric backscatter signal it is possible to detect clouds and connect this information to the simultaneously measured relative humidity. Open questions concern humidity inside cirrus clouds (Peter *et al.*, 2006): How could supersaturation with respect to ice arise inside cirrus clouds? Why does the expected relaxation to equilibrium not occur? With matched balloon soundings, it is possible to confirm or reject not only the occurrence, but also follow the evolution of high supersaturation. The gap between the two soundings is closed by microphysical box modelling. For more detailed information about the whole research plan see Peter and Spichtinger (2008).

The present diploma thesis is established in the very beginning of LAMMOC and accomplishes the task of trajectory modelling in order to forecast launching locations, times, and flight paths of the match balloon soundings.

1.2 Physical background

1.2.1 Cirrus clouds

A general way to group clouds is based on the classification system introduced by Luke Howard (1772–1864). It takes into account the height of the cloud's lower limit and their appearance. Concerning altitude low, middle, and high level clouds exist. Cirrus clouds are high level clouds above 6 km. They are typically thin, have a fibrous appearance, and shine white. Another way to group clouds is by physical properties like their particulate composition. In this case, differentiation is done between water clouds, ice-crystal clouds, and mixed clouds, with cirrus clouds as cold clouds composing of aspherical ice particles (Lynch, 1996).
Both heterogeneous and homogeneous freezing of particles lead to formation of cirrus clouds. In the presence of solid aerosol particles, such as soot, mineral dust or biological particles, heterogeneous ice nucleation may take place (DeMott *et al.*, 2003). Temperatures below $-40\,^{\circ}\mathrm{C}$ and high supersaturation are preconditions for homogeneous freezing of pure liquid solutions, as investigated in laboratory studies, e.g. by Koop *et al.* (2000). In ice supersaturated regions (ISSR), the potential formation regions of cirrus clouds, these conditions are given. Inside ISSR a continuous range from clear air via sub-visible and thin to optically thick cirrus clouds is possible. The different properties of their appearance may have opposite effects on the global radiation budget: Thick clouds induce a cooling effect while optically thin clouds lead to a warming. The latter let shortwave radiation pass through but absorb longwave radiation (Fusina *et al.*, 2007).
Based on surface observations, Warren *et al.* (2007) published an annual average cloud coverage of 22 % of high level clouds over land. Their horizontal and vertical distribution can also be observed by remote sensing systems like e.g. the Cloud-Aerosol Lidar with Orthogonal Polarization (CALIOP) aboard the Earth-orbiting Cloud-Aerosol Lidar and Infrared Pathfinder Satellite Observations (CALIPSO) satellite. Using this information, Nazaryan *et al.* (2008) analysed the horizontal and vertical distribution of cirrus clouds from June 2006 to June 2007. A total occurrence frequency of 16.7 % was observed on global scale averaged over one year, with 15.2 % coverage allocated to day- and 18.3 % to night-times. Sassen *et al.* (2008) and Nazaryan *et al.* (2008) agree in their latitude-longitude distribution of frequency. Cirrus clouds occur most often over equatorial central South America, western Africa, Indonesia, and the west-central Pacific Ocean in the 20° S to 20° N latitude band. Nazaryan *et al.* (2008) determine a maximum occurrence frequency of 94 % for multilayer cirrus clouds near the tropics in the 100° E to 180° E longitude band. Minima in cirrus cloud observations are at high polar regions as well as over deserts. Significant amounts of cirrus clouds lie in the midlatitude regions. Considering vertical extensions, Giannakaki *et al.* (2007) observed them generally in altitudes between 8.6 to 13 km in the midlatitudes. More precisely Nazaryan *et al.* (2008) identified the maximum

occurrence frequency of the cirrus base at 8 km and cirrus top at 11 km in this area. This is the altitude range at which the match technique is aiming.

1.2.2 Balloon soundings

The first known attempt to launch an unmanned balloon equipped with scientific, self registering instruments was initialised by Gustave Hermite in 1892 (Labitzke and van Loon, 1999). His balloon was made of silk, had a constant volume, and with its payload weight and lifting capacity the balloon was able to reach an altitude of about 9 km. Loss of gas, through the open neck of the balloon and by diffusion through its skin, induced the slow descent with the consequence of an enormous drift of the balloon with the wind. Richard Assmann developed an elastic balloon made of one piece of rubber and had the first successful launch on 1st February 1901. The rubber of the balloon expands during the ascent due to the decreasing air pressure and therefore the volume of the gas inside increases. Heights up to 20 km could be reached, the balloon bursted at top, and the instruments returned to ground on a parachute. Another important development was the application of a balloon-borne radio transmitter in the late 1920's to receive data during the flight and not just a few days later after the recovery of the instruments. The French scientist Robert Bureau coined the term "radiosonde", which refers to "any balloon-borne instrument capable of measuring parameters of interest at various altitudes and radioing this information to a receiver-recorder on the ground" (Bud, 1997).
Since then the network of stations launching balloons became more and more dense and many national weather services started to use this method. Today there are balloon soundings at several hundred stations all over the world (Oolman, 2009). Many of them perform regular radio-soundings at 00, 06, 12, and 18 universal time coordinated (UTC).
An advantage of radiosondes compared to remote sensing instruments are in situ measurement results of the atmosphere, recorded with high frequency and accuracy. The vertical profile of a balloon sonde shows the present situation of all different air layers. While e.g. light detection and ranging (LIDAR) systems are limited by the cloud cover, the radiosonde can pass through this layer and record data inside as well as above clouds.

1.3 Establishment of the match technique

Since the discovery of the Antarctic "ozone hole" in 1985 (Farman *et al.*, 1985), ozone studies in the Arctic were enhanced, too. In this context, the idea of the "match technique" was first published by Rex (1993) and von der Gathen *et al.* (1995). Within the European Arctic Stratospheric Ozone Experiment (EASOE), 26 ozone sounding stations

formed a dense network in the northern winter of 1991 to 1992. Single balloon soundings were linked by tracing the encountered air parcels along their horizontal and vertical motions in the atmosphere. A successful match describes two launches with balloon-borne instruments probing the same air mass at different times. Ozone depletion rates caused by chemical conversion could be calculated from changes in ozone concentrations between two matched soundings. The polar vortex, which arises during the winter polar night and forms a strong circumpolar wind in the middle to lower stratosphere, is a key ingredient to polar ozone loss since it isolates the enclosed air. It provides a basis for the formation of photochemically active products during the polar winter and the rapid destruction of ozone when the sun comes up and the polar vortex dissipates (Finlayson-Pitts and Pitts, 1999). The measurements following the evolution along the trajectories inside the polar vortex were first based on random matches. During further campaigns in the winter 1994/1995 and 1995/1996 the match technique was improved by an active forecasting tool, which allowed to trigger the second sounding at a predicted, optimised time instead randomly at one of the four UTC standard times (Rex, 1997; Rex *et al.*, 1997, 1999).
Outside the polar regions other published match approaches are not known. Balloon calculation tools available on the Internet, e.g. from the University of Wyoming (`http://weather.uwyo.edu/polar/balloon_traj.html`) or by Rick von Glahn (`http://www.eoss.org/wbaltrak/`), are just for computation of one single balloon track. Beyond these available tools, the present work developed a new tool suited for the design of sonde matches. The new tool aims at high precision matches by allowing the time and location of the second launch to be optimised with respect to the first launch. While this approach should have the best merits in terms of precision, it clearly requires a mobile team to perform the matching second sounding.

2 Material and Methods

At the beginning of Chapter 2, details about starting locations and the payload configuration of recent and prospective match balloon soundings are presented. With regards to the computational work, Section 2.3 contains basic principles of the trajectory modelling and a detailed description of the developed forecasting match tool.

2.1 Study sites

All balloon launches are planned within Switzerland, an alpine country in the middle of Europe. The total area amounts to 41 285 km^2 with a maximum extension from north to south of about 220 km and from west to east of 348 km. A topographic map of Switzerland is included at a later point in Figure 2.6 on Page 16.
The MeteoSwiss radio-sounding site at Payerne (46.813° N and 6.943° E) is taken as fixed starting point for one of the two matched soundings. Payerne is located in the western part of Switzerland where MeteoSwiss runs an aerological station including their sole radio-sounding site. Four operational weather balloons are launched per day, two of them measure vertical profiles of temperature, dew point, and wind, the other two detect just wind profiles. The starting time of the match balloon sounding has to be positioned within the time span between two operational soundings. The collaboration with MeteoSwiss allows to benefit from their infrastructure as well as their manpower.
Within the greater area of Zurich, a mobile team performs the matching second sounding. Zurich is located approximately 135 km northeast from Payerne. As the prevailing wind direction in Switzerland is southwest, Zurich is most of the time downstream of Payerne. The IAC at ETH Zurich (47.379° N and 8.549° E) is equipped with all necessary instruments for balloon soundings on the roof of the institute building and also has the possibility for mobile soundings, respectively.

2.2 Measurement equipment

2.2.1 Balloon sonde

The measuring system for the balloon sonde is composed of equipment described in the following sections. It utilises a Swiss radiosonde including a global positioning system (GPS) receiver. The Swiss radiosonde measures the meteorological parameters temperature, pressure, water vapour with a hygristor, as well as wind extracted from the GPS data. The data are received online during the flight by an antenna, a broadband communications receiver. The balloon, which carries the payload of approximately 1800 g, is filled with helium or hydrogen. The amount of gas is chosen to reach a mean rate of ascent of $5\,\mathrm{m\,s^{-1}}$. The balloon itself consists of elastic rubber which expands during the ascent because of the decreasing air pressure causing the volume of the gas inside to increase. The balloon bursts typically at altitudes between 30 and 35 km, and the payload returns to the ground on a parachute. Either the payload carries details for a potential finder or it will be recovered actively in order to use it again. To this end a TWIG locater can be added to transmit the final coordinates in mountainous terrain, where receiving GPS data with an antenna is impossible.

2.2.2 COBALD backscatter sonde

Radiation on its way through the atmosphere is scattered and absorbed by gases and particles. The operation of the compact optical backscatter aerosol detector (COBALD) is based on this principle to characterise aerosol and cloud particles. COBALD has been engineered at ETH during the last four years as a follow up development of the backscatter sonde by Rosen and Kjome (Rosen and Kjome, 1991). With 500 g total weight, it is much lighter than its parent which is important as it can thus be flown without special permission, i.e. simple information of air traffic control (ATC) of a forthcoming launch suffices. So far the instrument is designed for applications during night time only as solar radiation saturates the photodetector. With a frequency of typically 1 Hz, a detector measures the backscattered light from two light emitting diodes (LED), a blue one with a wavelength of 455 nm and an infrared one whose wavelength is 870 nm. The detector is placed between the two LEDs with the optical axes aligned in parallel. Overlap between the emissions and the detector's reception fields of view is established at a distance of 0.5 m. Since the detected light decreases with the square of the scattering region distance, a range approximately of up to 5 m is probed by the sonde.
Scattering and absorption of light by spherical particles is mathematically described by Mie theory. In addition to this accurate solution of the electrodynamical scattering prob-

lem, there exist approximate expressions. Depending on the wavelength λ of the scattered light in relation to the particle diameter D, these expressions are valid in certain asymptotic cases. The scattering of particles with $D \ll \lambda$ is called Rayleigh scattering. Gases scatter light by Rayleigh scattering, which is also known as molecular scattering. For $D \sim \lambda$ the scattering is called Mie scattering. Much larger particles, which are classified as $D \gg \lambda$, constitute the third category of geometric scattering (Finlayson-Pitts and Pitts, 1999; Seinfeld and Pandis, 2006). Besides Rayleigh scattering aerosol and cloud particles induce the Mie scattering. Using light of two different wavelengths, COBALD is able to distinguish between Rayleigh and aerosol scattering and accordingly between clear and cloudy air.

Signals of backscatter sondes are shown as backscatter ratio (BSR), which can be expressed by the net signal divided by the Rayleigh signal:

$$BSR = \frac{Aerosol + Rayleigh\,Signal}{Rayleigh\,Signal}\,. \tag{2.1}$$

In regions of pure molecular scattering the BSR is unity. This value, depending on the air density known from measured temperature and pressure, depends on the characteristics of each individual sonde and requires a calibration. The reference sonde, a calibrated sonde of the Rosen and Kjome type, is therefore run simultaneously to a COBALD sonde over night with low atmospheric aerosol loading. The calibration value for COBALD can be extrapolated from the reference sonde by correlating sonde signals arising from the natural aerosol variability.
The aerosol backscatter ratio (ABSR) is – analogous to the BSR – the aerosol signal divided by the Rayleigh signal:

$$ABSR = \frac{Aerosol\,Signal}{Rayleigh\,Signal}\,; \tag{2.2}$$

$$ABSR = BSR - 1\,. \tag{2.3}$$

The ABSR is needed for calculation of the colour index (CI), which is defined as the ratio between the ABSRs at two wavelengths:

$$CI = \frac{ABSR\,(870\,nm)}{ABSR\,(455\,nm)}\,. \tag{2.4}$$

Figure 2.1 results from Mie theory calculations with an index of refraction for ice ($n = 1.31$). Assuming the angular means of the backscattered light and a certain standard deviation for the mode of the lognormal size distribution it is possible to conclude the particle radius from CI. Small particles have a CI of 1 which increases with rising particle sizes. At

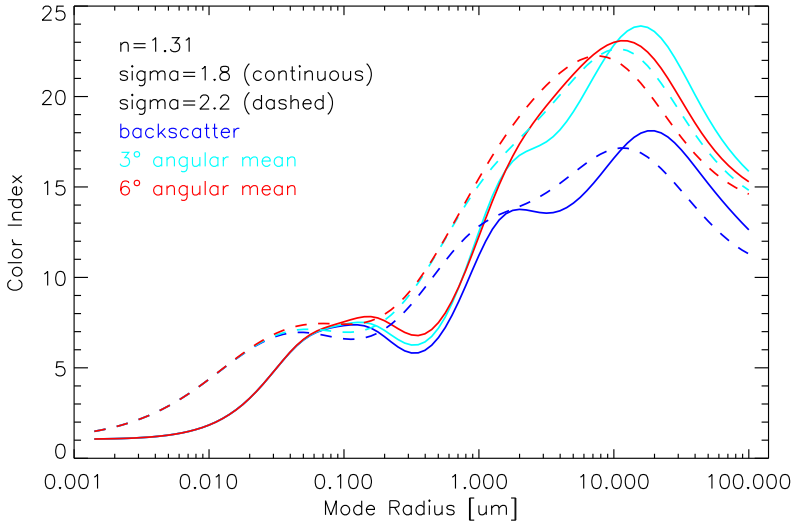

Figure 2.1: Expected colour index as a function of particle radii assuming a refraction index of 1.31 for lognormal size distributions. Standard deviations and angular means are typical values for COBALD.

particle radii larger than 3 µm the extracted information becomes more and more uncertain because of the Mie oscillations in the CI, and for this reason the measurement provides only the information that the particles have radii larger than 3 µm, but not by how much. Both angular means are typical for COBALD, compensate Mie oscillations and are close to each other up to particle radii of 3 µm.

2.2.3 Snow White hygrometer

The Snow White hygrometer developed by Meteolabor AG of Switzerland is suited to measure water vapour concentrations in the atmosphere on radiosondes with high precision. Its functional principle is a dew point mirror. The dew point T_{dew} is the temperature to which air temperature T_{air} must be cooled to be saturated with respect to a plane surface of water. Similarly, the frost point T_{frost} defines the corresponding temperature with respect to ice. Both cooling processes take place at constant pressure. A mirror is cooled by a Peltier element. Due to this the air above becomes saturated and on the mirror dew or frost condensate forms. Illuminated by a lamp variations in the reflected light caused by changes in the condensate thickness are detected via an optical fibre by a phototransistor. The power of the Peltier cooler is adjusted automatically to keep this signal constant at a level of 80 % of the uncoated, clean mirror. The temperature of the mirror indicates the dew or frost point temperature of the air (Vömel *et al.*, 2003; Fujiwara *et al.*, 2003).

The instrument has two known drawbacks:

1. In extremely dry layers of air, when the dew point or frost point is more than 22 K lower than ambient air temperature, the single Peltier stage does not suffice to provide the necessary cooling and therefore the condensate on the mirror evaporates (manufacturer estimate for $-80\,^{\circ}$C given in Fujiwara *et al.* (2003)). Thus, no measurement is possible within these layers, and whether or not the instrument managed to rebuild an appropriate condensate layer after leaving the dry layer must be judged from the data after the flight.

2. The instrument keeps being troubled by electronic oscillation problems.

While the first drawback is a principal tradeoff for simplicity and lightweight, the second problem is currently worked on and will hopefully be eliminated in future sonde generations.

Based on T_{air} and T_{frost}, both measured with the Snow White hygrometer, it is possible to derive the relative humidity over ice, RH_{ice}. Due to the fact that on cirrus level T_{air} is between $-20\,^{\circ}$C and $-50\,^{\circ}$C, the following equations are given with respect to ice.

RH_{ice} is defined as the ratio of vapour pressure e to the saturation vapour pressure e_{ice}:

$$RH_{ice} = \frac{e}{e_{ice}}\,. \tag{2.5}$$

At frost point temperature the vapour pressure is equal to the saturation vapour pressure

$$e = e_{ice}(T_{frost}) \tag{2.6}$$

and therefore RH_{ice} can be written as

$$RH_{ice} = \frac{e_{ice}(T_{frost})}{e_{ice}(T_{air})}\,. \tag{2.7}$$

The dependency between e_{ice} and T is described by the Clapeyron equation. The following formula by Murphy and Koop (2005) provides a high accuracy approximation of the Clapeyron equation:

$$e_{ice}(T) = \exp\!\left(9.550426 - \frac{5723.265}{T} + 3.53068\ \ln(T) - 0.00728332\ T\right). \tag{2.8}$$

In Formula 2.8 the temperature unit is Kelvin and the pressure is in Pascal.

2.3 Modelling of match balloon soundings

The model which has been programmed and evaluated during this diploma thesis is built on a balloon trajectory model developed by H. Wernli and M. Sprenger. The trajectory computation of a balloon track is done inside the three-dimensional grid of a numerical weather prediction (NWP) model (Section 2.3.1) in a Lagrangian specification (Section 2.3.2). The wind fields needed for the kinematic trajectory calculation as well as the pressure, temperature, and the water vapour mixing ratio are provided by different NWP models. At each grid point of the NWP model information of the atmospheric conditions is quantified. Within the grid box values are derived by linear interpolations of the values stored in such grid points (Section 2.3.2). Thus the distance between two grid points in horizontal and vertical direction influence the quality of the resulting trajectory.

2.3.1 Numerical weather prediction models

"Numerical weather prediction is the technique used to forecast the weather by computer from its present, measured state up to several days ahead." (European Centre for Medium-Range Weather Forecasts, 2009). The initial model conditions result from observed data from radiosondes, weather satellites, and surface observations of the present weather. Besides the available observations, data assimilation comprises a previously computed forecast referred to as first guess (Lorenc, 1986). The change of atmospheric quantities from their current values to the future is expressed in mathematical equations. These equations describe a variety of physical laws (e.g. conservation of energy, transformation of phase, black body radiation), which can be solved only approximately. The calculations are performed on a three-dimensional grid, where the vertical level spacing is inhomogeneous in order to better resolve the low level atmospheric conditions (Pielke, 2002).

Depending on the planned balloon launch time the programme's trajectory calculation bases on one of three NWP models, whose temporal domain is sketched in Figure 2.2. Whereas forecasts of the Consortium for Small-Scale Modelling (COSMO) are short-range, the European Centre for Medium-Range Weather Forecasts (ECMWF) provides medium-range weather forecasts. All models focus on Europe and the spatial domain for each NWP model can be seen in Figure 2.3.
Calculations more than three days ahead rest upon forecasts produced by ECMWF. The whole atmosphere around the globe needs to be included in a model for medium-range forecasts. Two times every day a new prediction is available reaching up to ten days into the future with a horizontal resolution of 25 km $\times$ 25 km and 91 vertical layers rising up to 0.01 hPa which is about 80 km altitude (European Centre for Medium-Range Weather Forecasts, 2009).

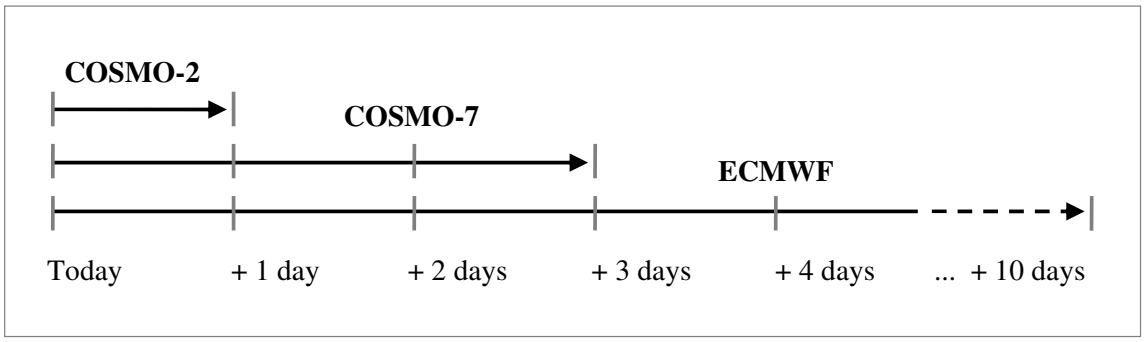

Figure 2.2: Temporal domains of the NWP models COSMO-2, COSMO-7, and ECMWF.

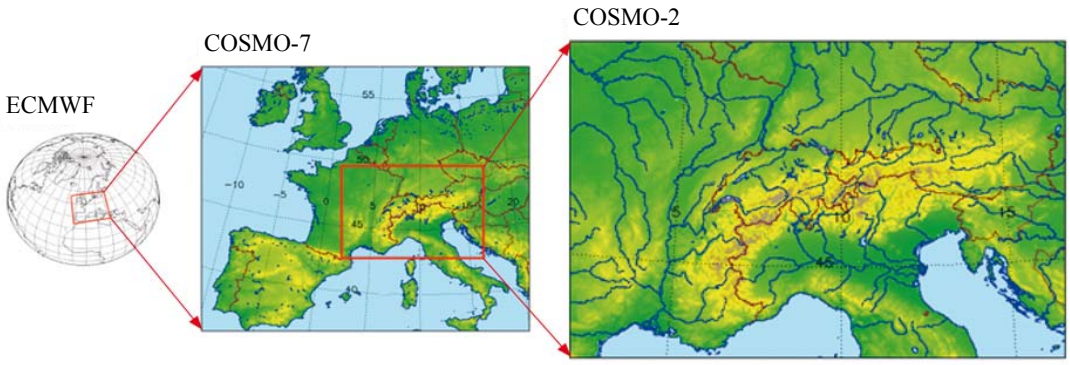

Figure 2.3: Spatial domains of the three nested NWP models. The ECMWF operates a global model describing the synoptic scales. MeteoSwiss operates the regional scale COSMO-7 and the local scale COSMO-2 models (Source: Federal Office of Meteorology and Climatology MeteoSwiss, 2009).

Organised in an international framework COSMO runs a short-range forecasting model (Consortium for Small-Scale Modelling, 2009; Steppeler *et al.*, 2003). MeteoSwiss is one of the participating meteorological services and considers this model as its "most important forecasting tool for the short-range period of one to three days into the future" (Federal Office of Meteorology and Climatology MeteoSwiss, 2009). Two versions of COSMO are operated at MeteoSwiss, COSMO-7 on regional scale and COSMO-2 on local scale. The lateral boundary fields for COSMO-7 are provided by the ECMWF model, the analogue fields for COSMO-2 are in turn provided by COSMO-7. Both COSMO models put Switzerland in its centre and cover the alpine region with a high resolution. The spacing between two grid points is 6.6 km for COSMO-7 and 2.2 km for COSMO-2, respectively. In vertical direction both models have the same 60 levels which reaches an altitude of approximately 23 km. A scale-dependant decay of terrain-features with height is implemented in COSMO by a smooth level vertical (SLEVE) coordinate (Schär *et al.*, 2002). COSMO-7 runs are performed twice a day for the next 72 hours. Eight times a

day, but only up to 24 hours in the future, COSMO-2 provides a forecast (Federal Office of Meteorology and Climatology MeteoSwiss, 2009).

2.3.2 Trajectory modelling

On the macroscopic scale all kinds of liquids and gases can be considered as fluids. There are two principle ways to describe fluids in motion. Focusing on points fixed in space and looking how a variable changes with time at that specific locations is known as the Eulerian point of view. In contrast, the development of a variable occurring when the observer follows an individual fluid parcel as it moves through space and time describes the Lagrangian perspective. The paths of these fluid parcels are called trajectories (Stohl, 1998).

According to Stohl (1998) a trajectory of a specific air parcel is described by the differential equation

$$\frac{dX}{dt} = v(X,t) \tag{2.9}$$

where X denotes the position vector of the air parcel, v the wind field, and t the time. The integral form is written as

$$X(t) = X(t_0) + \int_{t_0}^{t} v(X,t)dt\,. \tag{2.10}$$

The equations above are solved approximately by a finite-difference scheme for meteorological applications expanding $X(t)$ in a Taylor series. The original method by Petterssen (1956) is used as a variant in the Lagrangian Analysis Tool (LAGRANTO), developed by H. Wernli at ETH on the basis of ECMWF analysis and forecasts (Wernli and Davies, 1997; Stohl *et al.*, 2001). It was recently extended for the output of the NWP model COSMO and furthermore adapted to MATLAB routines for the balloon trajectory model by M. Sprenger. This version is used for match calculation. The method comprises a forward time step followed by a certain amount of iterations to estimate the air parcel's next position most precisely. The iteration number is indicated by superscripts. Starting at point $X(t_0)$ the first iteration of the next point $X^1(t_1)$ is calculated with the wind field v at point $X(t_0)$ and a forward time step Δt:

$$X^1(t_1) = X(t_0) + v\big(X(t_0)\big)\Delta t\,. \tag{2.11}$$

A disadvantage of Equation 2.11 is that it does not take the change in the wind field along

the pathway into account. Therefore, further iterations are calculated similar to Equation 2.11 using the mean wind between the starting point $X(t_0)$ and the arrival point of the last iteration $X^{i-1}(t_1)$:

$$X^i(t_1) = X(t_0) + \frac{1}{2}\Big[v\big(X(t_0)\big) + v\big(X^{i-1}(t_1)\big)\Big]\Delta t\,. \tag{2.12}$$

Typically three steps of iteration lead to adequate numerical convergence with real wind fields (Sprenger, 2006).

The required wind components at the locations between the grid points are derived from a linear interpolation of the grid values in four dimensions, the three spatial and the temporal dimension. Each wind vector has to be interpolated separately. Each 15 seconds a trajectory position is calculated internally, and one per minute is provided as output.

2.3.3 Calculation of single balloon soundings

To calculate a balloon track several pieces of input are needed. First the specification of the starting point with an exact definition of coordinates in latitude, longitude, and height above ground is required. COSMO-2 and COSMO-7 need the height in metres, ECMWF in pressure. The starting time with an accuracy of one minute must be set. Presently the balloon ascent is approximated by a fixed rate of $5\,\mathrm{m\,s^{-1}}$, which corresponds to several other balloon trajectory calculation tools e.g. at MeteoSwiss and Deutscher Wetterdienst (DWD). The descent, originally also implemented as a fixed rate of $-10\,\mathrm{m\,s^{-1}}$, was improved by M. Heidemann and replaced by a table of empiric velocities depending on altitude (Heidemann, 2009). The point of burst is about 30 km height, but differs slightly from balloon to balloon and is therefore set to an estimated value of 10 hPa. Because of the limited vertical extent of the COSMO fields the programme switches to the atmospheric conditions of the ECMWF NWP model during every run above 20 km altitude. The last coordinate calculated before the trajectory crosses the upper boundary of COSMO is stored and set as a new starting point for the further calculation based on ECMWF fields. The balloon descent calculated with ECMWF is also interrupted at 20 km height to change back to COSMO.

2.3.4 Calculation of match balloon soundings

The new tool, implemented in MATLAB, provides the opportunity to combine two balloon flights to a match flight with the task of finding the best starting location and time for the

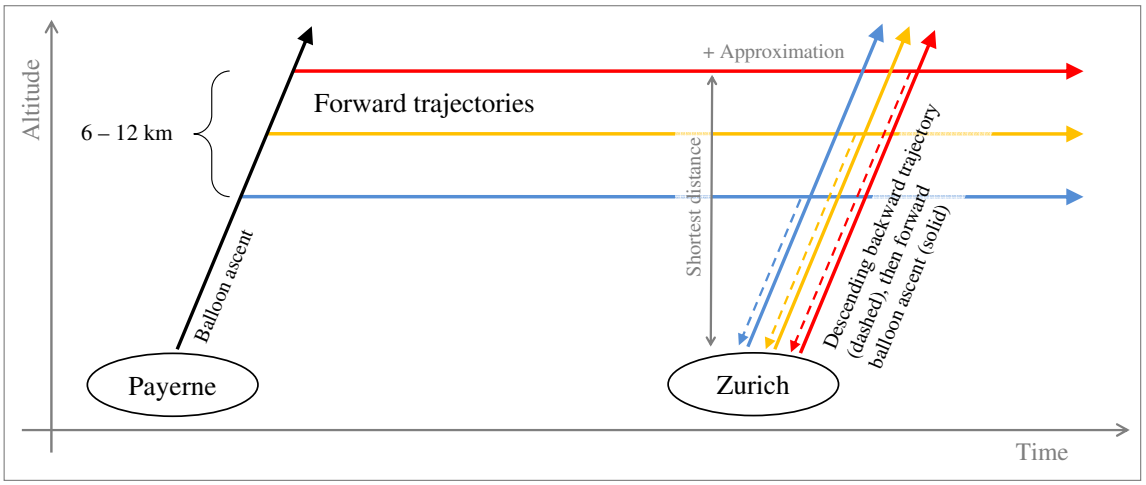

Figure 2.4: Sketch of the model's working steps with coloured arrows representing different trajectories.

mobile balloon start in the greater area of Zurich (Section 2.1). The schematic sketch of the model's work flow is illustrated in Figure 2.4.

The first programme step is the simulation of a single balloon flight as it is described in Section 2.3.3 with Payerne, the MeteoSwiss radio-sounding site, taken as a fix starting point. A certain number of air parcels on the balloon ascent trajectory of this flight is selected in the target height region between 6 and 12 km altitude. The choice of one air parcel per minute with a climbing rate of $5\,\mathrm{m\,s^{-1}}$ leads to a vertical distance of 300 m between the air parcels. For illustration only three example trajectories are shown in Figure 2.4, whereas the operational mode of the programme supports 15 air parcels. The computational procedure, used for the balloon's ascent, is adopted to calculate the way of the chosen air parcels through space and time. For this purpose the superimposed balloon rate of ascent is changed to zero. These air trajectories end either by leaving the horizontal area of the NWP model or by reaching the end of the time window of the NWP model. Next, for each trajectory of an air parcel a corresponding second balloon ascent is calculated. To clarify the connection between the air trajectory and the associated balloon ascent, the trajectory is called "balloon parent trajectory". To achieve the location and time of the second balloon launch, a descent with a vertical velocity of $-5\,\mathrm{m\,s^{-1}}$ is simulated backward in time. This backward balloon trajectory (dashed lines in Figure 2.4) describes the same pathway as the afterwards calculated forward ascent. The starting point and time of the second balloon, the mobile launching site, is equal to the coordinates at ground level. As an additional constraint, the second balloon should be as close as possible to Zurich. Therefore the shortest distance from the air parcel's trajectory to the IAC building is evaluated. To avoid that all starting points are located upstream of Zurich the air parcel's trajectory is followed from its closest position to Zurich for an empirical time interval. This time interval (called approximation in Figure 2.4) accounts for the vertical wind profile and constitutes half of the time needed for the balloon ascent up to the corresponding height. By iteratively adjusting the above-mentioned empirical time interval

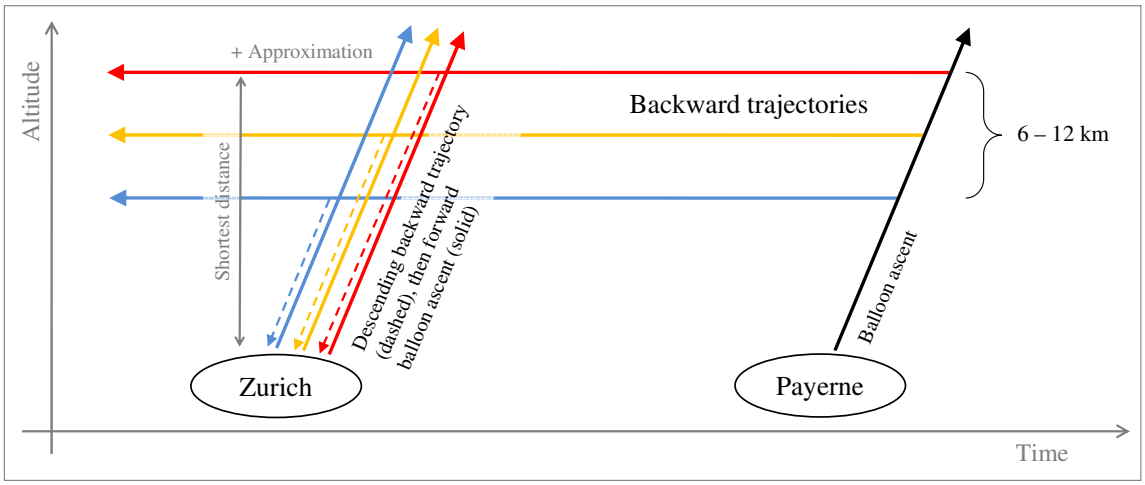

Figure 2.5: Sketch of the model's working steps – backward mode.

taking account of the corresponding wind speed, the launch position distance to the IAC can be minimised. The calculation results in 15 starting locations and corresponding times for a second balloon flight. In the forecast, each of these balloons match at least one of the forward-calculated air parcels that were previously sampled by the Payerne sounding, namely the air parcel on its parent trajectory.

In case the wind direction is to the west, the balloon start in Payerne has to be scheduled after the mobile sounding and accordingly the model is run in a backward mode. Figure 2.5 illustrates this case with the same programme steps as in eastward direction. The balloon flight of Payerne is still simulated first, though the trajectories are calculated backward in time.

To obtain information of meteorological parameters it is possible to trace the trajectories again for extracting the selected parameter. By this temperature [°C] and specific humidity [kg kg^{-1}] can be specified from the NWP along the trajectories. Conversion to potential temperature [K] is included in the model as well as to relative humidity [%] and mixing ratio [ppm]. Wind speed [m s^{-1}] and wind direction [deg] are calculated from latitude and longitude time series.

Match criteria

The given meteorological situation is judged to be favourable for a match launch by the following criteria. All of them should be fulfilled for at least one of the 15 calculated possible balloon ascents.

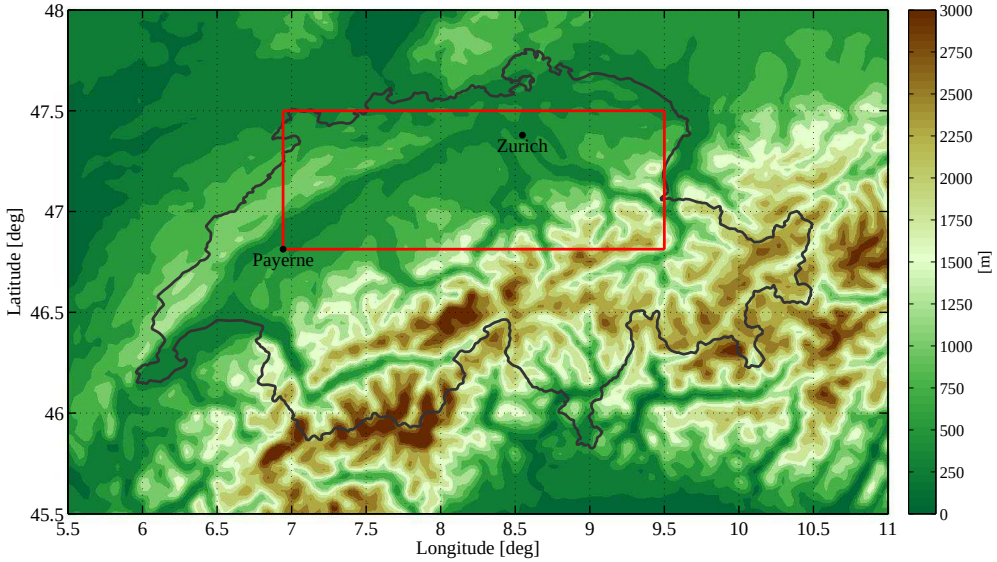

Figure 2.6: Topographic map of Switzerland. The rectangle defines the area for mobile match balloon launches referring to the first match criterion.

1. Within Switzerland starting points of mobile match balloons conducted in collaboration with MeteoSwiss, Payerne, have to be positioned inside the red rectangle of Figure 2.6. Accordingly, the trajectories have to cross this red rectangle. Wind directions from 0–90° as well as from 180–270° fulfil this criterion. For northeastern winds the programme can be run in the backward mode with Payerne as the second starting point described in the prior section. Also in this case we refer to the marked area. The starting point of the mobile launching is required to be within the Swiss border. The northern border is in the vicinity of 47.5° latitude and is therefore set as northern boundary in the programme. Beside that, the topography of Switzerland defines the southern boundary. In mountained terrain the probability of losing the radio contact to the balloon is too large.

2. The match distance criterion as depicted in Figure 2.7 assesses the influence of wind shear on the match quality. Wind shear describes a difference in speed or direction between two layers of air in the atmosphere. Three-dimensional distances of all potential second balloon ascents to all given air trajectories are calculated at the same point in time on isentropic surfaces. Henceforth, these distances are called “match distances”. Distances between two points are always calculated by their given geographic coordinates. The distance between two longitudes is variable and taken into account by determining longitudes as function of latitudes. The left side of Figure 2.7 shows how these match distances are calculated. The position of the balloon is compared to each forward trajectory. The encircled numbers mark points in time.

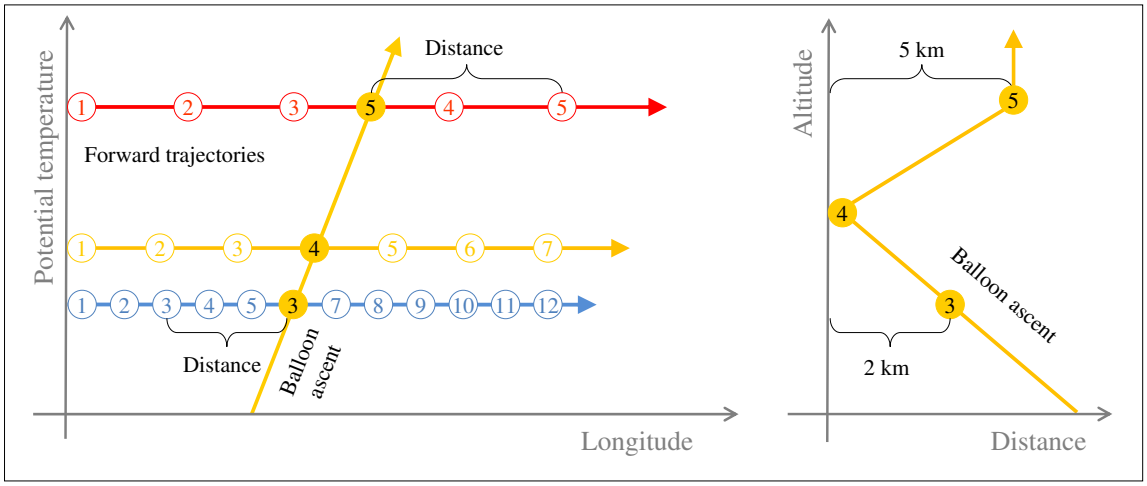

Figure 2.7: Match distance criterion to evaluate wind shear. The three-dimensional distance between a balloon ascent and each calculated forward trajectory is taken at the same potential temperature and point in time. The encircled numbers mark points in time, and identical numbers mark the same times.

At point three in time the balloon trajectory (yellow arrow) crosses the potential temperature level of the air trajectory marked by a blue arrow. The distance between the balloon and the air parcel at that point is 2 km. At a later time the balloon reaches the position from which its backward balloon trajectory calculation was started. Consequently the match distance between the balloon trajectory and its parent trajectory, describing the pathway of the target air parcel, is zero. The sketch shows larger wind speeds on higher altitudes. When the balloon and the red air parcel have the same isentropic surface the red air parcel is transported further. The existing match distance is marked in the coordinate system on the right hand side of Figure 2.7. The axis are equal to those that the model outputs. The criterion is defined as the maximum match distance over a range of approximately 2 km height. The match distance has to be smaller than 20 km. Large distances indicate strong wind shear. Under special conditions with a clear hint of e.g. a supersaturated region between 6 and 12 km height, it might be worth to execute a flight, anyway. The goal for the flight carried out is to achieve the target air parcel with less than 10 km distance. In the modelled forecast this distance is zero.

3. The elapsed time between two launches should be at least one hour. This time span of one hour is assumed to be needed to observe possible changes in supersaturation in the probed air mass.

4. For match flights within LAMMOC a predicted relative humidity close to 100 % inside the altitude region of interest is assumed as an indicator for the occurrence of cirrus clouds.

Section 3.2 provides a tabulation on how often these criteria are fulfilled during spring and summer 2009.

Model operation and output

The daily 00 UTC forecasts from ECMWF and COSMO-7 as well as the 06 UTC forecast from COSMO-2 are readily prepared at 09 UTC. Automatically each morning (installed as a Unix "crontab") the match model calculates the results for the current and the next four days in advance.

Data from every calculation are written to text files. Information on latitude, longitude, altitude, pressure, temperature, potential temperature, water vapour mixing ratio, relative humidity over ice, wind speed, and wind direction for each trajectory or pathway of a balloon flight is stored every minute. Additionally latitude, longitude, and altitude data build a keyhole markup language (KML) file for visualisation in Google Earth as in Figure 2.8. All corresponding figures of Chapter 3 are produced automatically during the model run. They visualise the different match criteria for the final evaluation of the situation by the user.

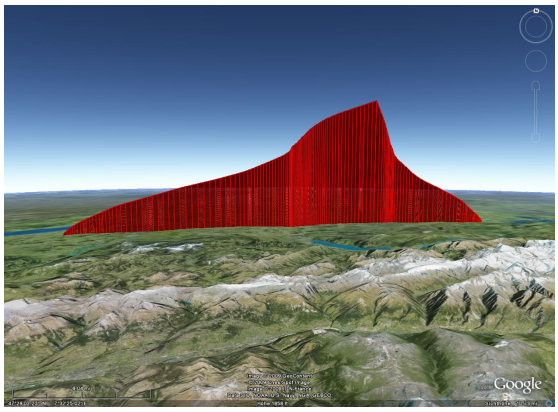

(a) Typical single balloon flight starting from Payerne (starting point left) with a definite buoyancy of $-5\,\mathrm{m\,s^{-1}}$, an expected point of burst at 10 hPa, and an estimated rate of descent.

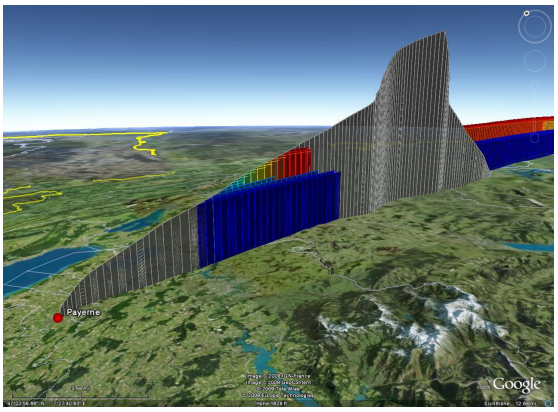

(b) Initial sections of the forward air trajectories. Their air parcels are detached during the simulated balloon ascent shaded in grey. Between 6 and 12 km altitude one air parcel per minute is encountered and a new trajectory is drawn. The colour code of the air trajectories symbolises height with lower trajectories in bluish and upper trajectories in reddish colours.

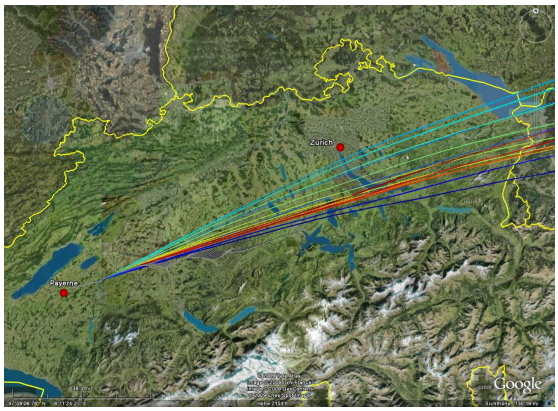

(c) Pathway of the forward air trajectories.

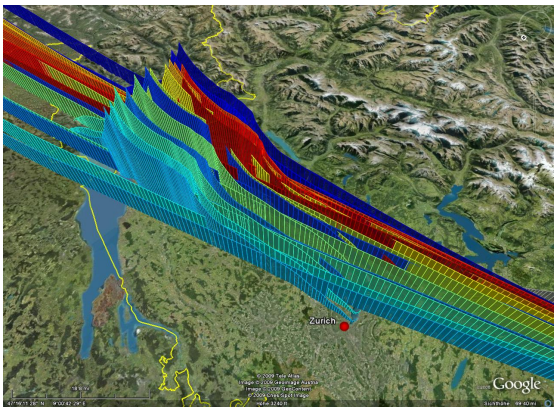

(d) All possibilities for a second balloon track, which will cross at least its target air trajectory.

Figure 2.8: Examplary model output of a match balloon sounding displayed in Google Earth.

3 Results

This chapter presents several results of model outputs. Section 3.1 illustrates the variability of weather situations which fulfil none, some or all criteria for a successful match. Representative examples are chosen to explain the evaluation process of the calculated forecasts. Systematic interpretation of daily weather forecast from 1st April to 31st August 2009 allows to assess the probability of favourable weather situations for match flights. This conclusion is presented in Section 3.2. The main part of this chapter (Section 3.3) analyses the realised match sounding which was accomplished during the night from the 6th to the 7th July 2009.

3.1 Exemplary model results

All calculations presented in this section are based on COSMO-2 and ECMWF forecasts. The used ECMWF forecast is computed at 00 UTC, whereas the COSMO-2 forecast, due to more frequent operational runs per day, is taken from 06 UTC of the corresponding day.

The overview of different model results starts with Figure 3.1 for the 22nd April 2009. The trajectories constitute the pathways of air parcels released during the simulated balloon ascent in Payerne forward in time. The colour code for the trajectories represents their order of heights with lower trajectories in bluish and upper trajectories in reddish colours. In Figure 3.1 the wind direction, which serves as the first quality criterion (Section 2.3.4), disqualifies the 22nd April and the further analysis of that example becomes needless. While the desired wind directions are from the northeast or southwest, in the present example wind from northwest carries the balloon launched at Payerne deeply into the Alps.

The 8th August, presented in Figure 3.2, gives another example for a weather situation unsuitable for a match flight. Figure 3.2(a) shows southwestern winds, which meet the first requirement. This time the figure is supplemented by a small window showing the allocation of the starting points for the calculated balloon launchings close to Zurich. As in the main picture the axes' units of the inset are degrees of longitude and latitude. A black

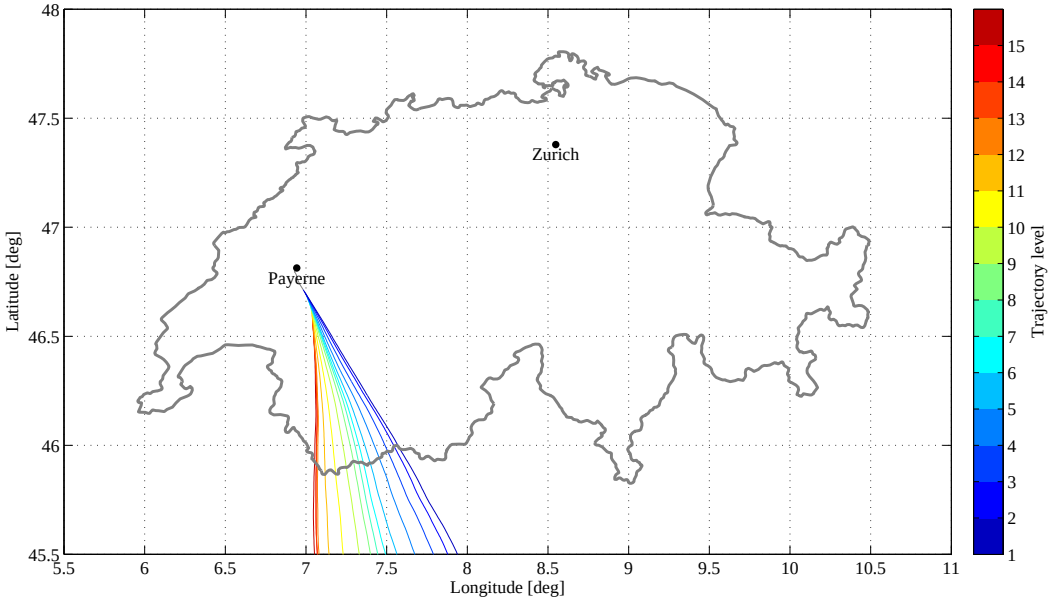

Figure 3.1: Model result of the 22nd April 2009. Forward trajectories for different altitude levels depicted in geographic coordinates refer to air parcels released during the simulated balloon ascent in Payerne. The colour code indicates the order of heights with lower trajectories in bluish and upper trajectories in reddish colours. The vertical distance between two adjacent trajectories is 300 m.

rectangle in the main figure denotes the inset's margin within Switzerland. Figure 3.2(a) is complemented by the Figures 3.2(b) and 3.2(c). They both show vertical profiles of the balloon trajectories started at the points depicted in the inset of Figure 3.2(a). Each balloon trajectory belongs not only to one starting point but also to one trajectory of Figure 3.2(a). As the colour code of Figure 3.2(a) indicates altitude, for Figures 3.2(b) and 3.2(c) it establishes the relation to the trajectory level as the same colour is taken for the profile of the balloon aiming to the corresponding trajectory. This use of the colour code is also obvious in the three-dimensional view presented in Figure 2.8(d). Figure 3.2(b) provides information about the predicted relative humidity with respect to ice evaluated from the COSMO-2 forecast data on the various balloon ascents. Figure 3.2(c) illustrates the distances between the different balloon ascents to all trajectories of Figure 3.2(a). Each cross represents one calculated distance between the balloon track and one trajectory of Figure 3.2(a) at the same potential temperature and time. This distance is zero on the balloons target trajectory level.

Though the wind direction in Figure 3.2(a) fulfils the first match criteria (Section 2.3.4), the horizontal wind shear is strong. This can be already seen in the trajectories' drift and the location of the starting points, which disperse over nearly one degree in latitude and longitude. Figure 3.2(c) demonstrates the consequences arising out of wind shear. The match distances are in case of the 8th August large and exceed the second examination of less than 20 km distance over 2 km altitude range. Figure 3.2(b) predicts the relative humidity trend in the upper troposphere. Listed as the fourth match quality criterion the relative

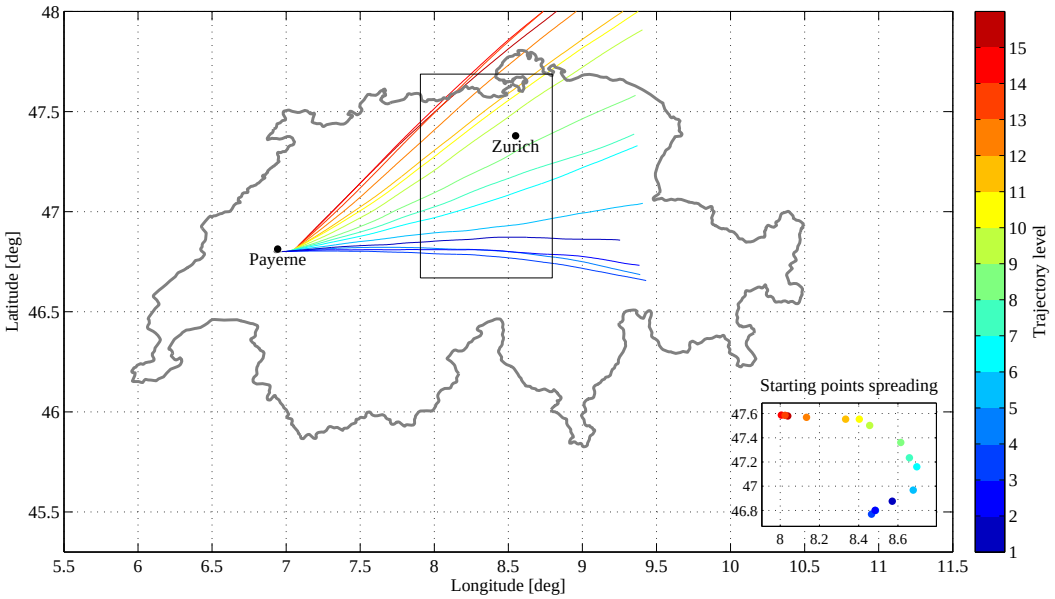

(a) Forward trajectories for different altitude levels. As in Figure 3.2(a) air parcels are released during the simulated balloon ascent in Payerne. The colour code indicates the order of heights with lower trajectories in bluish and upper trajectories in reddish colours. The vertical distance between two adjacent trajectories is 300 m. For each trajectory one possible balloon ascent is calculated and its starting point is displayed in the inset.

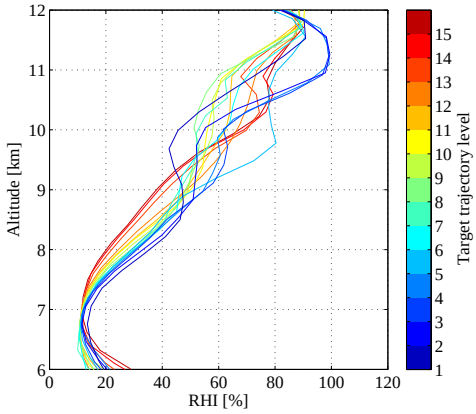

(b) Vertical profiles of calculated match balloon trajectories showing the relative humidity with respect to ice. The colour code of the balloon trajectories indicates affiliation to the forward trajectories of Figure (a) identical with the target trajectory level.

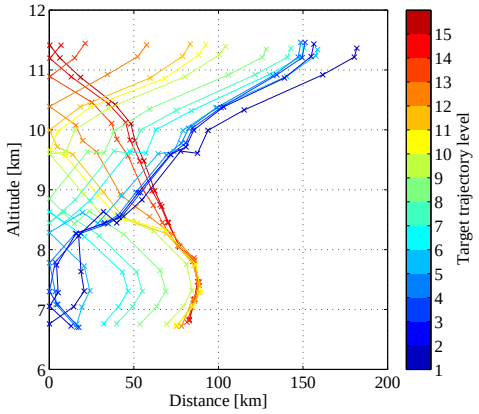

(c) Match distances between the calculated balloon trajectories and the forward trajectories displayed in Figure (a) at the same potential temperature level. At the balloon's target trajectory level the distance is zero.

Figure 3.2: Model result of the 8th August 2009.

humidity is essential for the execution of balloon soundings in LAMMOC, because cirrus clouds are the overall interest. Without any chance of cirrus cloud existence during the night a flight would be meaningless. On 8th August the relative humidity is close to 100 % only for the bluish trajectories close to the tropopause. As the tropopause region is not the target level of the blue profiles, the match distance at this altitude is more than 150 km (Figure 3.2(c)). Nevertheless, the failure to comply the match criteria of wind shear means the day has been rejected.

The weather situation on 16th July shows another case which cannot be categorised as suitable for match soundings. The wind from southwest direction (Figure 3.3(a)) fulfils the first criterion. The starting locations of the matching flight are also relatively close to each other as depicted in the inset of the figure. But Figure 3.3(c) shows a rapid growing distance between the different balloon ascents from mobile launches to the air parcels followed from Payerne. Accordingly the vertical wind shear – this time in velocity, not in direction – is responsible for this feature. The mean wind speed of the lower trajectory, starting at 7.1 km altitude, is 12.8 m s^{-1}. With 30.3 m s^{-1} the average wind speed of the upper trajectory, starting height 11.3 km, is considerably larger. The associated Table 3.1 expresses these differences in the time lag between the starting times for the mobile balloons. The initial time for the fixed balloon start in Payerne is 20:00 UTC. While the first suggested mobile balloon with the lowest target trajectory level should be launched at 22:46 UTC, 2 h and 46 min after the time of the balloon start in Payerne, the starting time of the balloon belonging to the topmost trajectory is 1 h and 29 min earlier. For a balloon which aims for a match at 7 km it is impossible to approach air parcels also in higher altitudes. The different wind speeds on the trajectory levels result in long distances between the single air parcels.

The 8th June appears to be an example for a suitable weather situation. Almost the whole situation as shown in Figure 3.4 seems to fit the match criteria. The wind direction is southwest and the wind shear is acceptable, as the distances in Figure 3.4(c) are smaller than 20 km over a range of at least 2 km height. Only the three lowest balloon ascents with a target trajectory level of about 7 km constitute an exception which could be already expected after looking at their slightly different courses in Figure 3.4(a). Figure 3.4(b) predicts a relative humidity close to 100 % up to 10 km. Based on these pieces of information trajectories with a target level between 8 and 10 km could be of interest. However, a detailed look into further analysis shows that the elapsed time between the two launches is too short. In the second column of Table 3.2 the starting times for the mobile launches close to Zurich are listed. The starting time of the first balloon in Payerne was set to 20:00 UTC as always. With a time difference of less than one hour between both balloon starts the third match criterion is not fulfilled. Due to the short time interval a match flight on the 8th June would not be recommendable as no significant changes are anticipated.

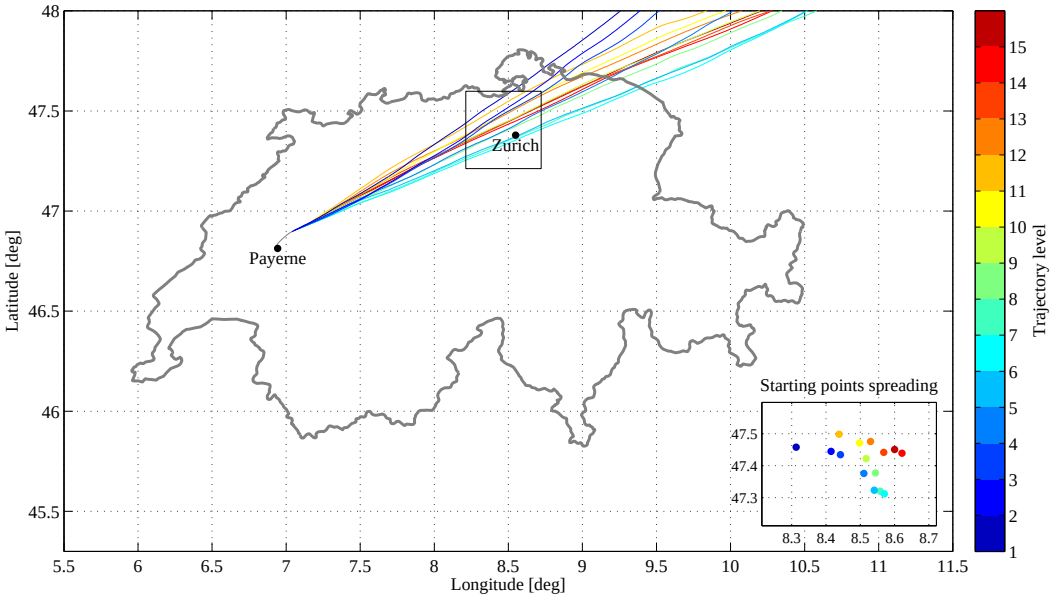

(a) Same as Figure 3.2(a).

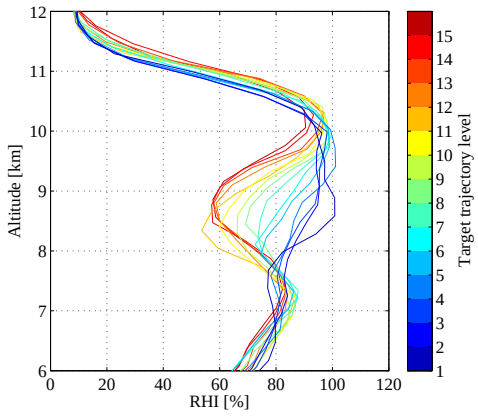

(b) Same as Figure 3.2(b).

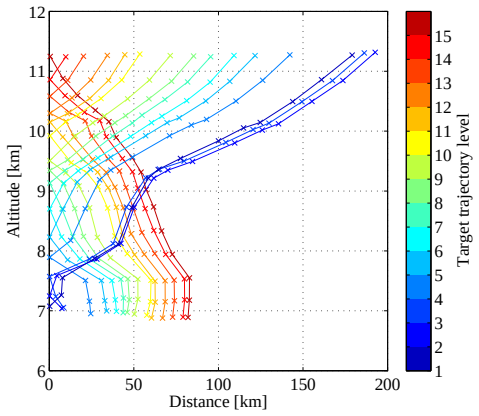

(c) Same as Figure 3.2(c).

Figure 3.3: Model result of the 16th July 2009.

Table 3.1: Starting locations and times for the second balloon on 16th July 2009. First balloon start in Payerne: 20:00 UTC.

Balloon trajectory	Starting time [UTC]	Starting location	
		Latitude [deg]	Longitude [deg]
1	22:46	47.458	8.313
2	22:59	47.445	8.415
3	22:56	47.434	8.442
4	22:30	47.376	8.511
5	22:19	47.323	8.541
6	22:12	47.312	8.570
7	22:03	47.320	8.558
8	21:59	47.377	8.544
9	21:51	47.422	8.517
10	21:42	47.471	8.498
11	21:35	47.499	8.438
12	21:33	47.476	8.530
13	21:26	47.442	8.568
14	21:22	47.439	8.622
15	21:17	47.451	8.600

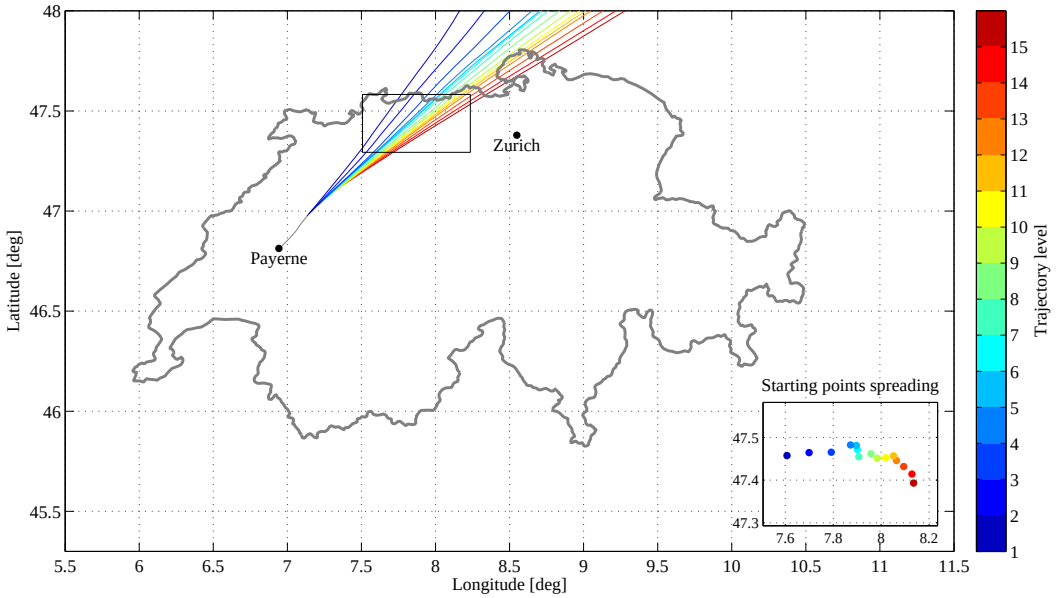

(a) Same as Figure 3.2(a).

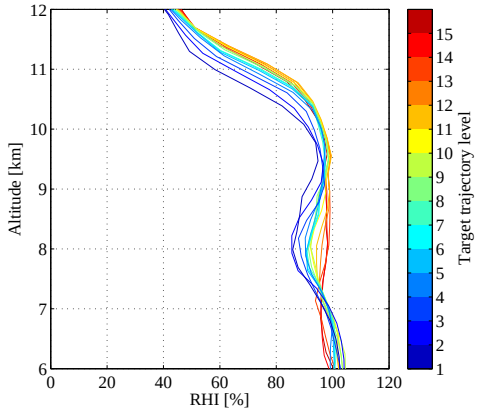

(b) Same as Figure 3.2(b).

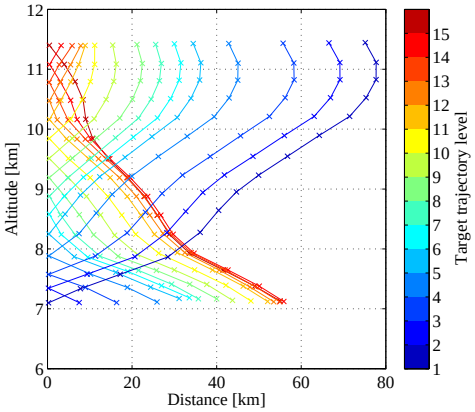

(c) Same as Figure 3.2(c).

Figure 3.4: Model result of the 8th June 2009.

Table 3.2: Starting locations and times for the second balloon on 8th June 2009.
First balloon start in Payerne: 20:00 UTC.

Balloon trajectory	Starting time [UTC]	Starting location	
		Latitude [deg]	Longitude [deg]
1	21:03	47.458	7.607
2	21:03	47.465	7.699
3	21:01	47.465	7.792
4	20:58	47.482	7.872
5	20:55	47.481	7.896
6	20:52	47.472	7.901
7	20:50	47.455	7.907
8	20:50	47.462	7.958

Balloon trajectory	Starting time [UTC]	Starting location	
		Latitude [deg]	Longitude [deg]
9	20:49	47.451	7.984
10	20:47	47.453	8.019
11	20:46	47.457	8.052
12	20:45	47.446	8.064
13	20:46	47.432	8.094
14	20:46	47.414	8.128
15	20:47	47.393	8.135

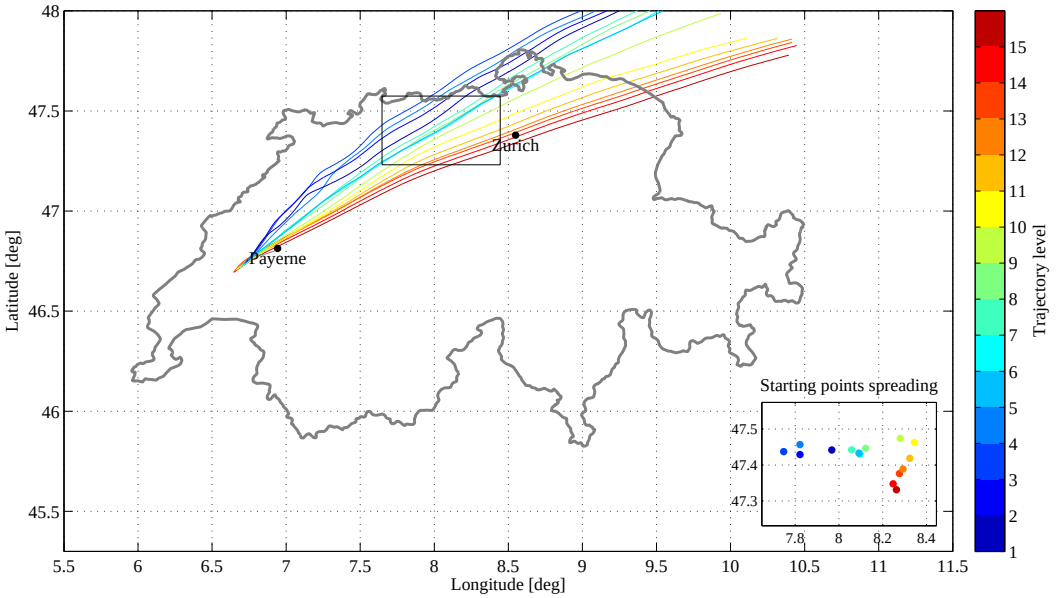

(a) Same as Figure 3.2(a), but for backward trajectories.

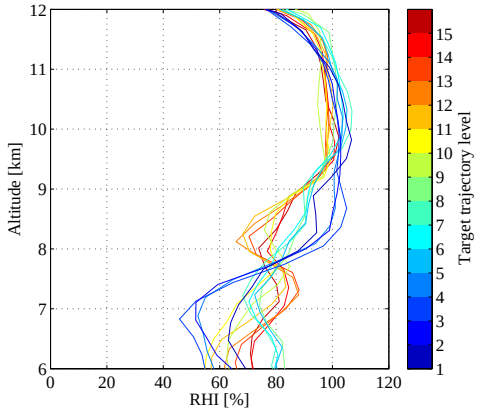

(b) Same as Figure 3.2(b).

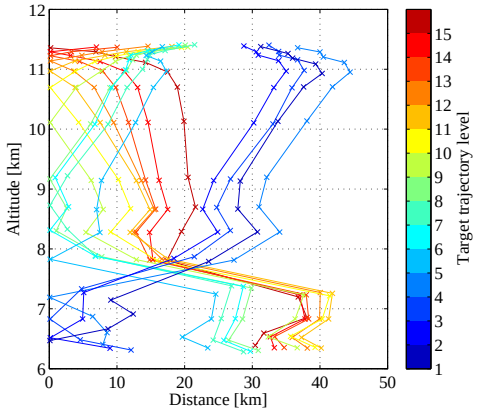

(c) Same as Figure 3.2(c).

Figure 3.5: Model result of the 23rd June 2009.

Table 3.3: Starting locations and times for the first balloon on 23rd June 2009. Second balloon start in Payerne: 22:00 UTC.

Balloon trajectory	Starting time [UTC]	Starting location	
		Latitude [deg]	Longitude [deg]
1	19:22	47.442	7.968
2	19:41	47.429	7.822
3	19:45	47.437	7.747
4	19:29	47.457	7.822
5	19:39	47.433	8.091
6	19:48	47.430	8.096
7	19:49	47.442	8.058
8	19:46	47.447	8.122

Balloon trajectory	Starting time [UTC]	Starting location	
		Latitude [deg]	Longitude [deg]
9	19:37	47.474	8.280
10	19:35	47.463	8.345
11	19:40	47.419	8.324
12	19:40	47.389	8.292
13	19:37	47.376	8.276
14	19:38	47.348	8.248
15	19:30	47.331	8.263

Figure 3.5 completes the set of examples of possible model results. The weather situation on 23rd June demands the backward mode and fulfils all match criteria. After an operational model run in forward direction on that day, the observed northeastern wind triggered a second model run computed backward in time. The balloon launch in Payerne is assumed for 22:00 UTC. The possible launch times for the mobile balloon range from 19:22 to 19:49 UTC (Table 3.3). Above 9 km altitude a relative humidity of 100 % is predicted in Figure 3.5(b) for all balloon trajectories. Figure 3.5(c) indicates that the distance criteria for trajectory number 5 to 15 is fulfilled, too. As these balloon trajectories belong to the trajectories more closely to Zurich they were favourable for a match balloon sounding.

A situation which fulfils all match criteria in forward direction is described in Section 3.3.

3.2 Probability of a favourable match situation

The probability of a favourable match situation is estimated from the number of days on which all match criteria specified in Section 2.3.4 are fulfilled. Each day's model output was judged by these criteria for the period from 1st April to 31st August 2009. Table 3.4 lists the total number of days which fail or meet the conditions separately for each month. Days which do not meet all of them are further divided by the single requirements. The numbers used in Table 3.4 for this purpose refer to Section 2.3.4.
One out of five days during the selected period was a favourable day for a match sounding with the focus on cirrus clouds. Altogether, 153 days were evaluated during spring and summer 2009 and 32 of them met all criteria for the realisation of a match sounding. A match sounding without special cloud requirements was possible during 45 days which suits to 30 % of the days reviewed. Often there were several days in a row with good potential for match flights. In May, for example, stable high pressure weather conditions were responsible for twelve consecutive days with southwest wind and low wind shear. Nine of them promised also relative humidities close to 100 % in the target region. In general, the major cause for disqualification is a failing of the wind direction criterion. Days are excluded 7 % of the time due to wind shear and 11 % of the time due to the short time difference between the two soundings. Another 11 % is not of interest for LAMMOC with its focus on cirrus clouds. Examples for each case of failing are described in the previous Section 3.1 in detail.
On the one hand, 21 % of days had favourable match conditions within the evaluated period, while on the other hand the match sounding interpreted in the following Section 3.3 was the only one carried out. As match soundings within LAMMOC are organised in collaboration with MeteoSwiss at Payerne, this cooperation still had to be established and the

Table 3.4: Frequency of days which fulfil none, some or all of the match criteria: [1] Wind direction. [2] Wind shear. [3] Elapsed time between the two soundings. [4] $RH_{ice} \geq 100\,\%$. A day which does not fulfil criteria [1] and [2], for example, is listed under [1] only. For further specification see Section 2.3.4.

	Days	Criteria fulfilled	Criteria not fulfilled				
			[1]	[2]	[3]	[4]	Total
April	30	3	21	4	2	0	27
May	31	13	11	0	4	3	18
June	30	6	20	0	3	1	24
July	31	2	17	3	4	5	29
August	31	8	18	1	0	4	23
Total	153	32	87	8	13	13	121

time management needed to be harmonised. Limited human resources at the ETH Zurich complicated the finding of suitable dates additionally.

3.3 Performed match sounding

3.3.1 Forecast situation

Evidence for a match situation on Monday the 6th July was already given by forecasts computed with ECMWF and COSMO-7 a few days earlier. Server maintenance jobs in the morning of the 6th July did not allow to obtain the COSMO-2 forecast from 06 UTC as usual. As soon as possible the forecast was loaded and due to the advanced time the updated 09 UTC forecast was taken instead.
The sounding from Payerne was scheduled for 20:30 UTC. The first forecast presented in Figure 3.6 is based on the calculation of 15 possible locations and times for a mobile launch as described in Section 2.3 and displayed in Section 3.1. All required match criteria were fulfilled. The wind was from southwest (Figure 3.6(a)), the distances between the balloon trajectories and the considered air parcels did not exceed 20 km over a height range of 2 km (Figure 3.6(c)), the elapsed time between the assumed launches in Payerne and Zurich was more than one hour (Table 3.5) and cirrus clouds could occur between 8 and 9 km altitude as the relative humidity was about 100 % (Figure 3.6(b)).
The calculated starting locations were very close to the ETH IAC building in Zurich, because the trajectories crossed Zurich exactly. The included black dot in the inset of Figure 3.6(a) symbolises the ETH IAC building. Instead of choosing one of the options offered by the programme, it was decided to launch the balloon directly from the roof of

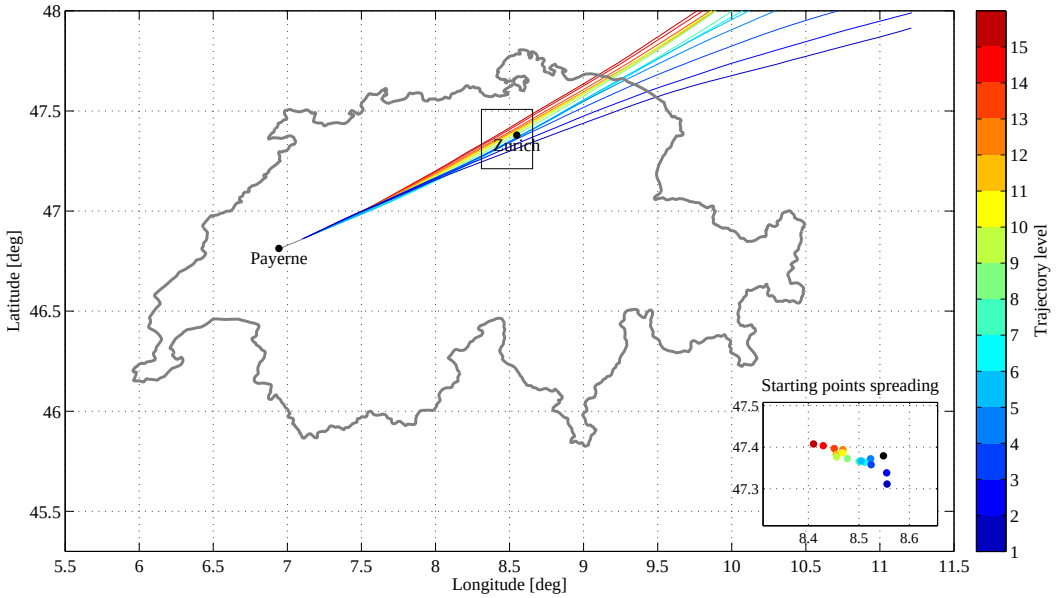

(a) Same as Figure 3.2(a). The black point in the picture's inset displays the ETH IAC building in Zurich.

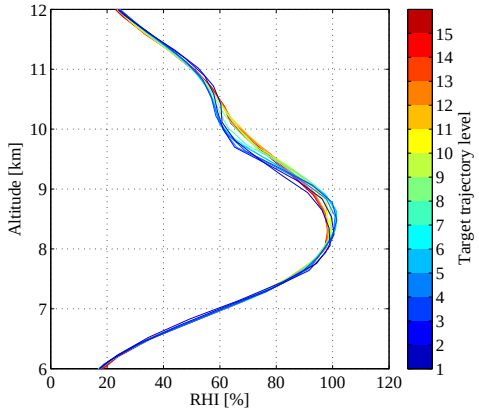

(b) Same as Figure 3.2(b).

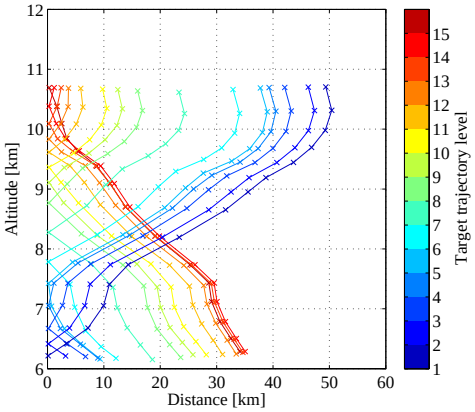

(c) Same as Figure 3.2(c).

Figure 3.6: Model result of the 6th July 2009.

Table 3.5: Starting locations and times for the second balloon on 6th July 2009.
First balloon start in Payerne: 20:30 UTC.

Balloon trajectory	Starting time [UTC]	Starting location	
		Latitude [deg]	Longitude [deg]
1	22:38	47.311	8.556
2	22:38	47.338	8.555
3	22:35	47.358	8.524
4	22:34	47.372	8.523
5	22:32	47.367	8.504
6	22:28	47.364	8.511
7	22:21	47.366	8.500
8	22:15	47.373	8.477

Balloon trajectory	Starting time [UTC]	Starting location	
		Latitude [deg]	Longitude [deg]
9	22:12	47.376	8.456
10	22:11	47.386	8.468
11	22:07	47.383	8.455
12	22:06	47.394	8.468
13	22:04	47.397	8.451
14	22:03	47.404	8.430
15	22:04	47.408	8.410

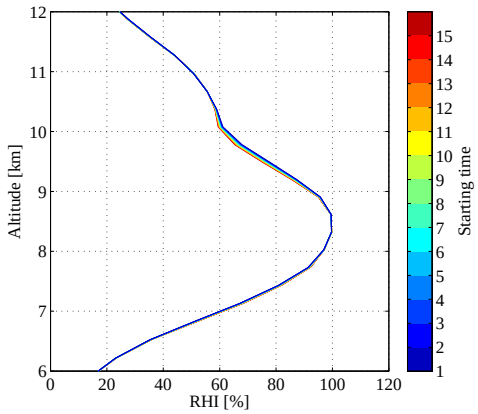

(a) Vertical profiles of calculated match balloon trajectories showing the relative humidity with respect to ice.

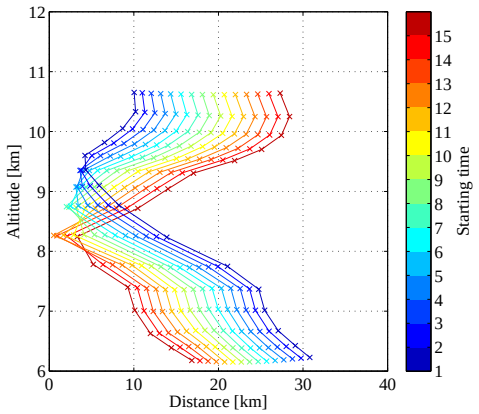

(b) Match distances between the calculated balloon trajectories and the forward trajectories displayed in Figure 3.6(a) at the same potential temperature level and point in time.

Figure 3.7: Modified model result of the 6th July 2009. The starting point for all simulated balloons trajectories are the coordinates from the ETH IAC building in Zurich. As the time is taken as variable parameter, the colour code in this modified case symbolises different starting times with earlier times in bluish and later times in reddish colours.

Table 3.6: Modified starting locations and times for the second balloon on 6th July 2009. First balloon start in Payerne: 20:30 UTC.

Balloon trajectory	Starting time [UTC]	Starting location	
		Latitude [deg]	Longitude [deg]
1	22:11	47.379	8.549
2	22:12	47.379	8.549
3	22:13	47.379	8.549
4	22:14	47.379	8.549
5	22:15	47.379	8.549
6	22:16	47.379	8.549
7	22:17	47.379	8.549
8	22:18	47.379	8.549

Balloon trajectory	Starting time [UTC]	Starting location	
		Latitude [deg]	Longitude [deg]
9	22:19	47.379	8.549
10	22:20	47.379	8.549
11	22:21	47.379	8.549
12	22:22	47.379	8.549
13	22:23	47.379	8.549
14	22:24	47.379	8.549
15	22:25	47.379	8.549

the institute's building. To find the best starting time, the programme code was adapted to the new situation. The coordinates from the IAC building were fixed and the time was implemented as a varying factor. Figures 3.7(a) and 3.7(b) were produced the same way as before yet at different times only instead of different times and locations. The characteristics of the lines in Figure 3.7(b) are therefore quite similar to each other with a shift of the shortest distance through heights. An early start induces a closer match in lower altitudes than a later start optimising distance for higher altitudes. Table 3.6 shows that the first balloon trajectory was modelled for a launch time 101 min after the start of the balloon in Payerne. The other balloon trajectories follow at intervals of one minute. The deviation from the locations suggested by the algorithm implies that the shortest distance to the air trajectories cannot be zero in any case. However, the additional distance of less than 5 km

in all cases was considered acceptable to improve starting starting conditions compared to the field. In case of the same starting locations for all balloon trajectories with just a change in time the relative humidity profile becomes more uniform as well (Figure 3.7(a)). With a time difference of 107 min between the two soundings the best match distance was prognosed to be 2 km at 8.7 km altitude. In the entire region above the distance was found to be smaller than 20 km (Figure 3.7(b)).

3.3.2 Analysis of the match flight

The launch of the balloon in Payerne was realised at 20:32 UTC, 2 min later than scheduled. The launch in Zurich was intended 107 min later. Effectively the second start occurred 105 min later at 22:17 UTC.
After the match flight, the model was rerun with corrected times using the COSMO-2 forecast as well as the COSMO-2 analysis available afterwards. The COSMO-2 analysis, which includes measured observations, gives the best estimate of the atmospheric conditions during the desired time (Federal Office of Meteorology and Climatology MeteoSwiss, 2009). For the validation of the match accuracy reached, the air parcels detached from the GPS balloon track in Payerne and followed via COSMO-2 analysis trajectories are compared with the GPS balloon track from the Zurich sounding. In addition, air parcels released on the GPS balloon track in Zurich were followed backward in time and compared to the GPS balloon track in Payerne. Comparing match distances obtained from forecast and analysis model outputs reveals the quality of the NWP forecast.

The modelled balloon tracks are compared with the recorded GPS during the flights. Figure 3.8 shows three cases, the deviation from the GPS track to the predicted COSMO-2 forecast balloon track and to the predicted balloon track from COSMO-2 analysis as well as the difference between both modelled balloon tracks. The deviation between two balloon ascents is defined as the absolute three-dimensional distance at the same point in time. Figure 3.8 is divided into two figures with Figure 3.8(a) illustrating the balloon ascent in Payerne and Figure 3.8(b) showing the situation in Zurich. The deviation is plotted versus the height for the first 20 km of ascent. The deviations in Payerne do not exceed 2 km, whereas both model trajectories differ extremely from the Zurich GPS track. For both locations the deviations between the modelled balloon tracks based on analysis and forecast data, respectively, are less than the deviations to the GPS tracks. The big discrepancies to the Zurich GPS track are found to be caused by different climbing rates. As described in Section 2.3 the model assumes as a fixed rate of ascent of $5\,\mathrm{m\,s^{-1}}$. Figure 3.9 provides the climbing rates as a function of height for the balloon flights in Payerne and Zurich clearly indicating that this assumption does not agree with the climbing rate observed for Zurich. Averaged over the first 20 km the mean climbing rate during the flight from Zurich was approximately $2\,\mathrm{m\,s^{-1}}$.

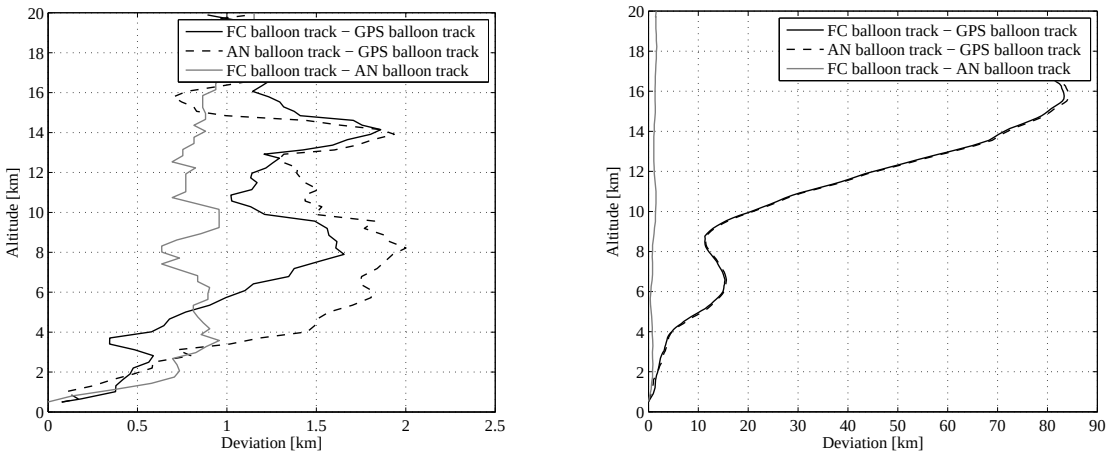

(a) Payerne (b) Zurich

Figure 3.8: Absolute deviations of computed balloon tracks with $5\,\mathrm{m\,s^{-1}}$ climbing rate to the corresponding GPS balloon track. The difference between COSMO-2 forecast (FC) and COSMO-2 analysis (AN) is additionally plotted in grey.

Erroneous filling of the balloon with not enough gas caused the slower than expected climbing rate of the balloon launched in Zurich. This change of conditions has to be accounted for a comparison of model and flight. Therefore the model was run once again, but now with a fixed climbing rate of $2\,\mathrm{m\,s^{-1}}$ for the second balloon. As plotted in Figure 3.10, the agreement is greatly improved as compared to the old climbing rate. The deviation is maximum 6 km, the distance between the forecast and analysis is somewhat bigger than using a climbing rate of $5\,\mathrm{m\,s^{-1}}$.

Figures 3.11 and 3.12 compare the match distances versus altitude to validate the match quality. For Zurich the model forecast with exact launch times and a balloon climbing rate of $5\,\mathrm{m\,s^{-1}}$ is plotted in contrast to a balloon with a climbing rate of $2\,\mathrm{m\,s^{-1}}$ in Figure 3.11(a). The balloon track with a climbing rate of $5\,\mathrm{m\,s^{-1}}$ is coloured in light blue to point out the relation to the same line of Figure 3.7(b) indicating there the balloon with launching time number five. In this case the shortest distance is predicted at 9.3 km height with 3.4 km distance to the air parcel of interest. Due to the reduction of the climbing rate to $2\,\mathrm{m\,s^{-1}}$ the shortest match distance becomes 2.2 km at an altitude of 7.8 km. The slower ascent delays the arrival of the balloon in the target region and thus causes the dislocation of the closest approach to the air parcels in lower altitudes.
To evaluate if the predicted match distance could be achieved, the match distances between the GPS data and the air parcels are calculated and presented in Figure 3.11(b). Several combinations are provided by this figure. Solid lines indicate the use of COSMO-2 forecast for the forward trajectories, dashed lines the use of COSMO-2 analysis. Each marker represents one calculated distance. Circles mark the distance from the trajectories to a GPS point, crosses the distance from the trajectories to the corresponding modelled

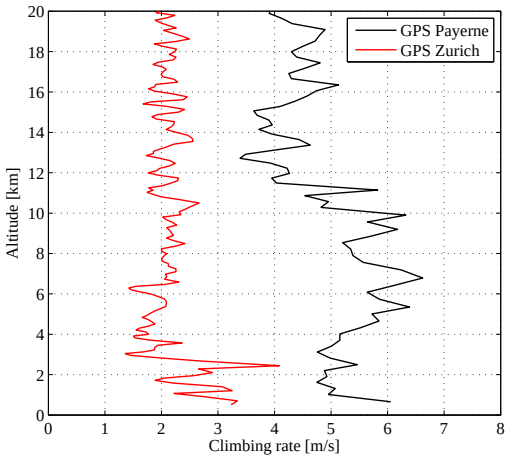

Figure 3.9: Recorded climbing rates of the balloon sondes started in Payerne (black) and Zurich (red).

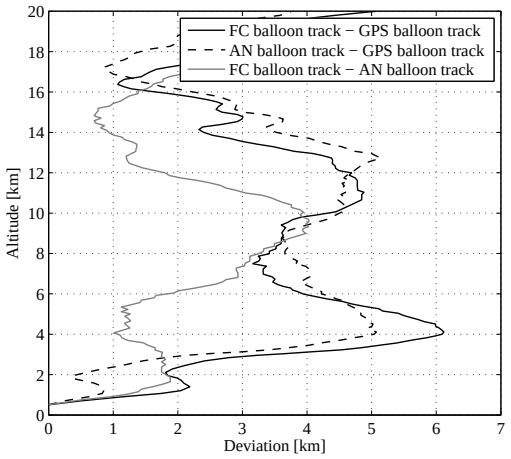

Figure 3.10: Absolute deviations of computed forecast (FC) and analysis (AN) balloon tracks with $2\,\mathrm{m\,s^{-1}}$ climbing rate to the GPS balloon track from Zurich.

balloon ascent based on the same NWP input. Thus a balloon ascent simulated using the COSMO-2 forecast is compared to the measured GPS data via COSMO-2 forecast trajectories only. The same applies for COSMO-2 analysis. In the forecast case the match distances between the trajectories and the GPS balloon track are similar in magnitude as the distances between the forecast trajectories and the corresponding balloon track simulation (solid lines in Figure 3.11(b)). The best match distance reached by the real balloon track is at 7.9 km altitude and counts 2 km distance to the forecast trajectories, 200 m better than predicted. The absolute difference between two corresponding match distances (both solid and both dashed lines, respectively, in Figure 3.11(b)) is comparable to the deviation between the balloon tracks (Figure 3.10). The same is observed by calculating the match distances with analysis data displayed in dashed lines. The deviation between the predicted and the observed balloon track causes the different match distances. The closest approach from the GPS balloon track to the COSMO-2 analysis trajectories is at an altitude of 7.6 km with 8.4 km distance.

Another possibility to verify the accuracy of the model is a match distance calculation in backward mode. The balloon launched in Payerne should match the air parcels traced back from Zurich with a similar error than the other way around. For this purpose 15 air parcels encountered on the GPS balloon track from Zurich are followed backward in time. The shortest distance to the GPS balloon track in Payerne is determined on isentropic surfaces for the same point in time and plotted versus height. Figure 3.12 shows a plot referring to the Payerne location similar to that in Figure 3.11(b). The GPS balloon track comes close to the COSMO-2 forecast trajectories at 8.3 km height with a distance of only 1.3 km (solid line with circle markers) whereas the COSMO-2 analysis trajectories are 9.3 km nearby to the GPS track at 8.5 km (dashed line with circle markers). It is noticeable that the

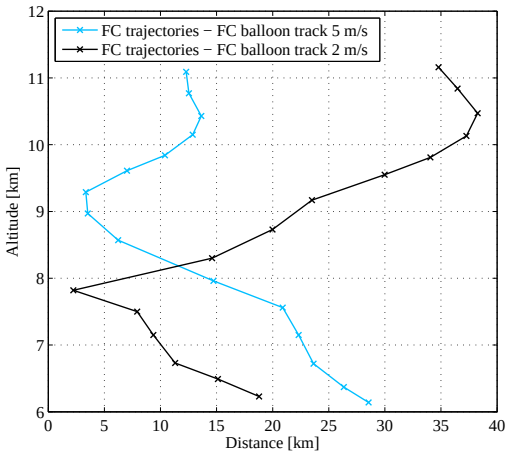

(a) Match distances between the calculated balloon trajectories and the forward trajectories computed with COSMO-2 forecast (FC) at the same potential temperature and point in time for $2\,\mathrm{m\,s^{-1}}$ (black) and $5\,\mathrm{m\,s^{-1}}$ (light blue) climbing rates.

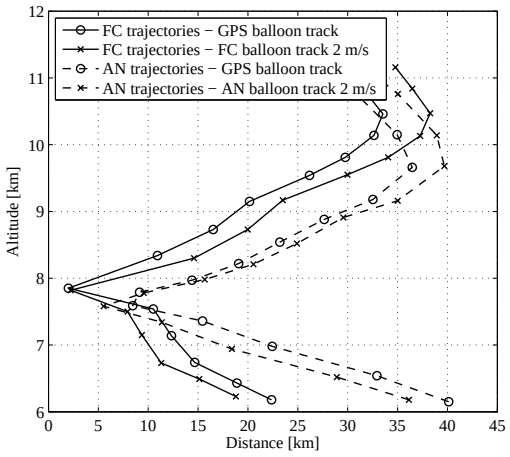

(b) Match distances between the balloon trajectories based on different datasets and the forward trajectories computed with COSMO-2 forecast (FC) and analysis (AN), respectively, at the same potential temperature level and point in time.

Figure 3.11: Match validation: Zurich.

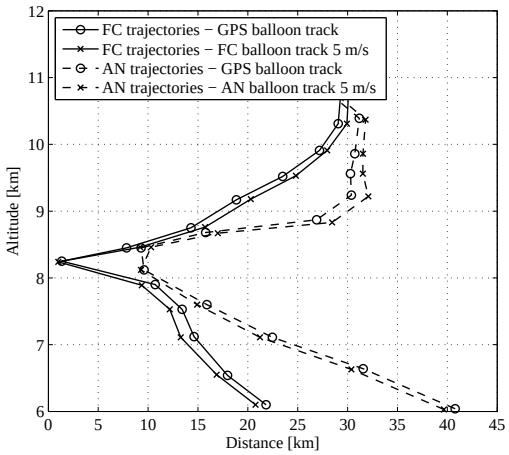

Figure 3.12: Match validation: Payerne. Match distances between the balloon trajectories based on different datasets and the forward trajectories computed with COSMO-2 forecast (FC) and analysis (AN), respectively, at the same potential temperature level and point in time.

altitude of the shortest distance in Payerne is slightly above that in Zurich. During its trip from Payerne to Zurich the air parcels descend by approximately 300 m and the potential temperature decreases about 0.5 K as indicated by both COSMO-2 forecast and analysis trajectories on the according altitude level. The deviations from the GPS match distances to the corresponding match distances of the forecast and the analysis, respectively, are small. In contrast, the disagreement between the match distances for the same balloon track is pronounced when different NWP inputs are compared. In Figure 3.11 and even more in Figure 3.12 this displacement between the solid and the dashed curves is obvious.

Slightly above 6 km altitude the match distances from the GPS balloon track to the forecast trajectories and the GPS balloon track to the analysis trajectories are more than 15 km away from each other. This deviation is likely to be caused by diverging air parcel trajectories between Payerne and Zurich depending on the model input – forecast or analysis – used.

Figure 3.13 shows the forecast and the analysis trajectories' course in four selected levels starting at the same time and point over Payerne. Trajectories computed with COSMO-2 forecast are drawn in solid lines, dashed lines represent COSMO-2 analysis as calculation input. To quantify the position error between the forecast and the analysis trajectories the absolute horizontal transport deviation (AHTD) versus time is given by Figure 3.13(b). Figure 3.13(c) supplemented the relative horizontal transport deviation (RHTD). The RHTD equates to the AHTD divided by the length of the trajectory (e.g. Riddle *et al.*

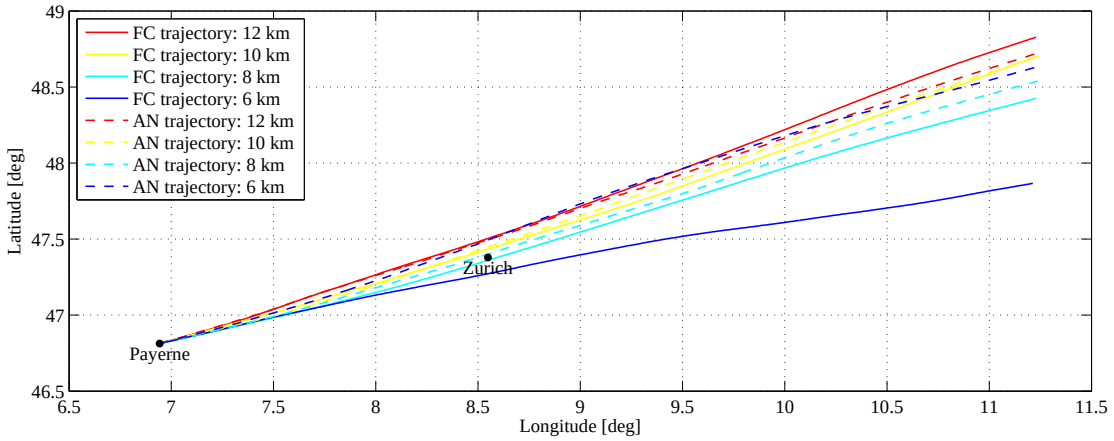

(a) Model trajectories of COSMO-2 forecast (FC) and analysis (AN) for the 6th July starting at 20:32 UTC.

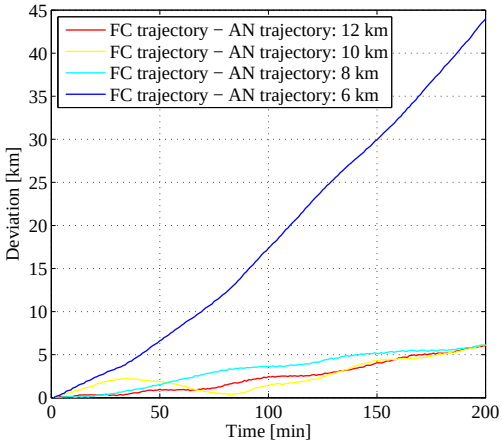

(b) Absolute horizontal transport deviation of the forecast trajectory to the analysis trajectory.

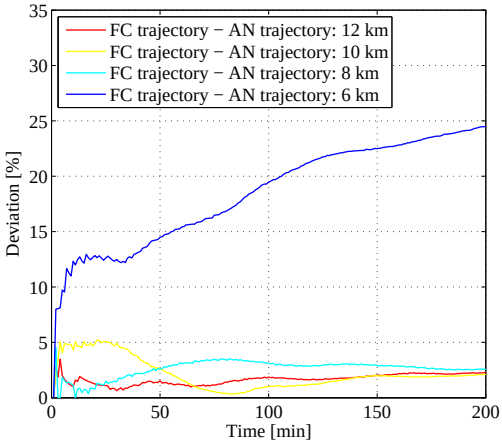

(c) Relative horizontal transport deviation of the forecast trajectory to the analysis trajectory.

Figure 3.13: Trajectory errors.

(2006)). Slightly different courses stand out for all levels in Figure 3.13(a), whereas at 6 km altitude the deviation is particularly large: The absolute horizontal distance amounts 8.4 km after one hour and adds up to 22.8 km after two hours of travel time. As fraction of the covered distance the relative deviation is about 15.4 % after one and 21.4 % after two hours. The deviations are due to wind speed and direction differences between forecast and analysis. After 120 min the wind speed differs about 2.4 m s^{-1} and the wind direction varies from 239 to 247°. Proceeding further in time the difference in wind direction becomes even larger.

The presented results and observed trajectory deviations are evaluated and discussed in the subsequent Chapter 4.

3.3.3 Measurement results

The recorded data of the COBALD sonde and the Snow White hygrometer during the flights in the night of the 6th July are presented as vertical profiles separately for Zurich and Payerne. The instrumentation is described in Section 2.2.
In Figure 3.14 T_{air}, T_{frost}, and RH_{ice} are a function of altitude. T_{air} decreases up to the tropopause continuously, which is in both graphs approximately at 11.5 km altitude. Above the tropopause T_{air} stays more or less constant at -50 °C until it increases again in the upper stratosphere. The profile of RH_{ice} is divided into two parts symbolised by two different shades of blue. *RH* is calculated for a liquid substrate on top of the mirror up to an air temperature of -25 °C. Within the temperature range from 0 to -25 °C the liquid condensate is supercooled and *RH* has to be defined with respect to ice. T_{frost} and consequently RH_{ice} data are partly defective. Between 7 and 11.5 km both Snow White feedback loops, used to control the mirror temperature, oscillated intensely during the flights.

The BSRs and the CI are displayed in Figure 3.15. The BSR colours are indicative of their λ drawn in blue and red. As in regions of pure molecular scattering the BSR is unity, the magnitude above this value is a sign for the presence of aerosol and cloud particles. The sonde launched from Zurich points out a low level cloud near 3 km (Figure 3.15(b)). A comparison to LIDAR data approves this observation. The used EZ LIDAR ALS450 from Leosphere was recently installed at the roof of the institutes building and is still in its test stage. Figure 3.16 shows the range corrected scattering signal obtained during the night of the match flight plotted as time-height cross section. Low level clouds are visible between 2 and 4 km altitude (e.g. between 21:40 and 22:40 UTC) by means of the stronger scattering signal and missing data above the cloud, which serves as a barrier for the laser light. The observation frequency of low level clouds above Zurich increased during the evening shortly after midnight local time. The Snow White hygrometer states *RH* of 90 %, which suggests an unstable cloud in the process of evaporation. In the profile

of Figure 3.15(b), the BSR increases again at 8.5 and 9.5 km and reveals a weak sandwich structure of a cirrus cloud. The LIDAR caught clouds at this altitude above Zurich as well. Unfortunately the data from the Snow White hygrometer are not usable to support the observation. The backscatter profile recorded from the sonde launched from Payerne demonstrates a clear sky up to the tropopause (Figure 3.15(a)). A small increase in the BSR indicates in both profiles the boundary between the troposphere and the stratosphere. Above the tropopause again an increasing BSR is observed in both profiles with a CI up to 5 only. The LIDAR visualises the same feature. As this occurs above the tropopause, where the Snow White indicates dry air, the evidence of cirrus clouds is excluded. The observed layer should consists of aerosols within the size range of 50 nm (Figure 2.1).
To summarise, there was clear sky in Payerne, while in Zurich clouds were detected by COBALD in two different heights. In a dry region above the tropopause a layer of small particles appeared on both flights. As the match height was below 8 km it is not possible to comment on the evolution of the clouds seen by the balloon borne instruments launched from Zurich.

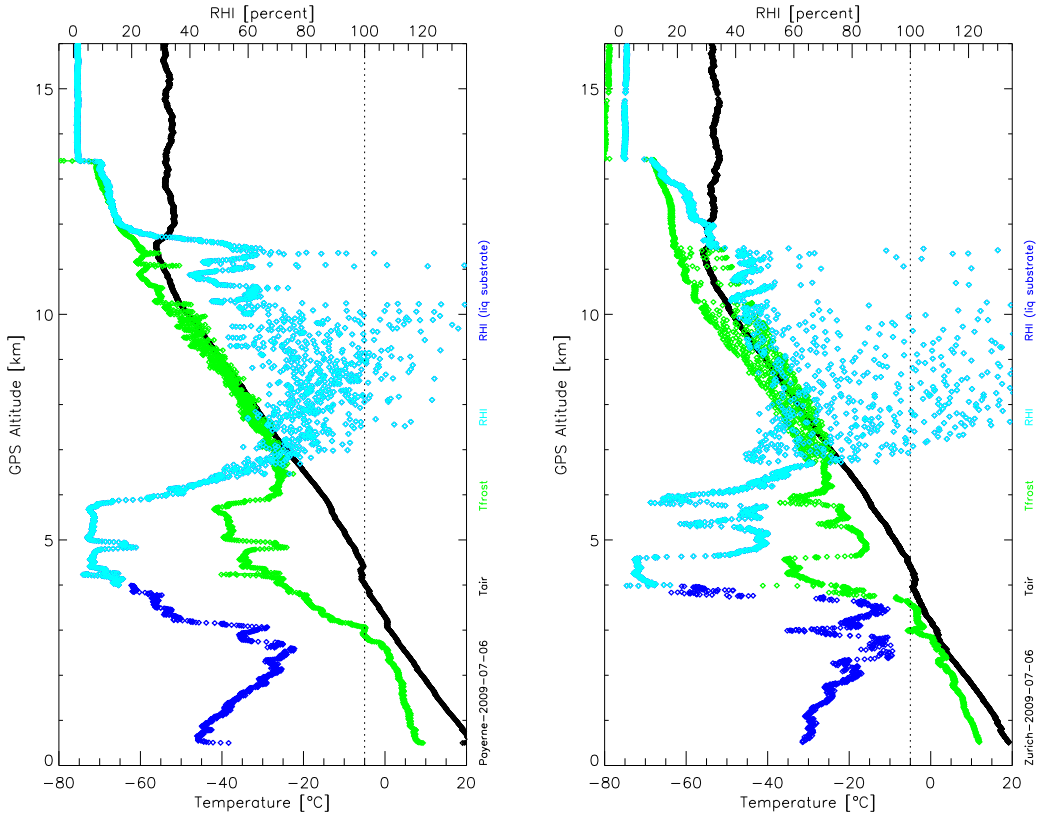

(a) Payerne (b) Zurich

Figure 3.14: Vertical profiles of the relative humidity with respect to ice (RH_{ice}) in cyan, the frost point temperature (T_{frost}) in green, and the air temperature (T_{air}) in black. The dark blue part of the RH_{ice} curve indicates the calculated profile for a liquid substance over the saturation vapour pressure with respect to ice.

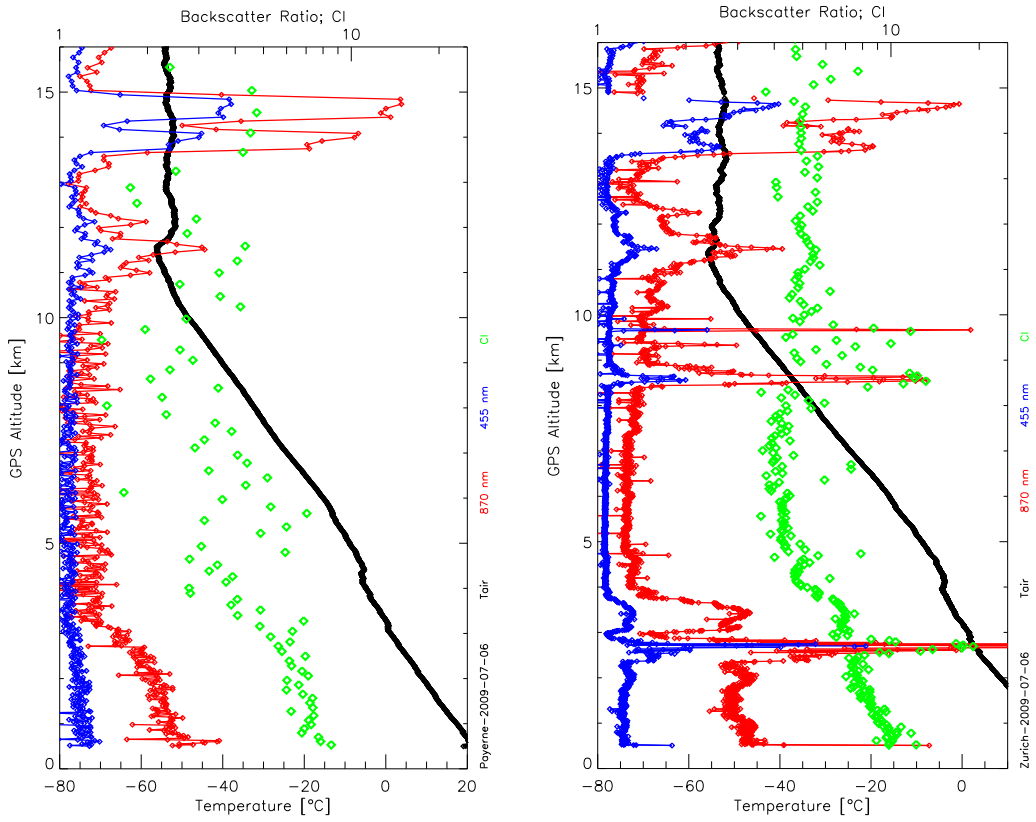

(a) Payerne (b) Zurich

Figure 3.15: Vertical profiles of the backscatter ratio (BSR) detected from COBALD with a wavelength λ = 455 nm in blue and λ = 870 nm in red. The colour index (CI) is included as green dots.

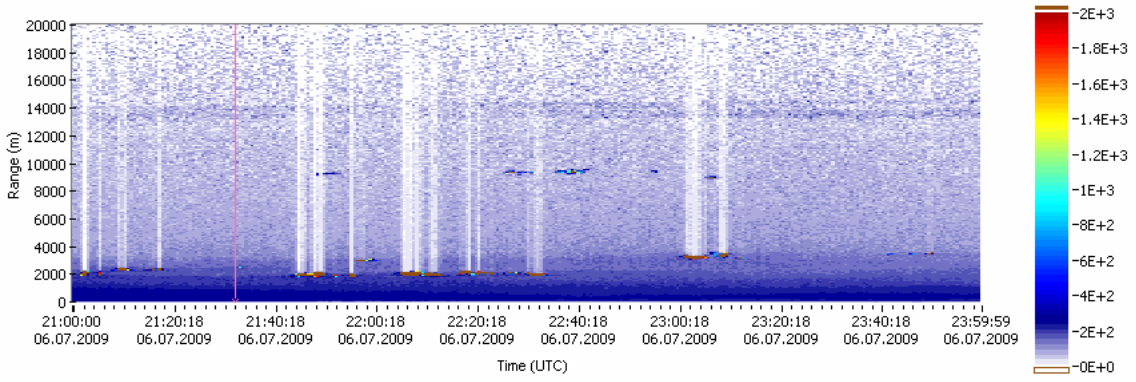

Figure 3.16: LIDAR scattering ratio plotted as time-height cross section.

4 Discussion and Conclusion

In the framework of this thesis, a forecasting tool to compute trajectories for match balloon soundings has been developed. A detailed description of the mode of operation and several exemplary outputs are presented. The findings of the single match flight carried out during this thesis are analysed in detail with respect to their agreement with the model. In this chapter, analysis results are discussed and conclusions for further work are drawn.

There is evidence that an erroneous forecast on 6th July is responsible for deviations between computed and recorded trajectories. To elucidate this statement, a discussion of the relevant model errors is given as follows. In addition to the wind field errors, Stohl (1998) and Seibert (1993) mention both truncation and interpolation errors as the most important error sources for the computation of kinematic trajectories. These different error sources of general nature are discussed with respect to their potential influence on the trajectory accuracy and thus also their final vitiation of the match accuracy.
Numerical truncation errors result from the approximation of Equation 2.10 that neglects higher order terms of the Taylor Series (Stohl, 1998). According to Walmsley and Mailhot (1983), the truncation error is dependant on Δt and can be reduced by choosing an accurate time step. Dividing the horizontal resolution of the used grid by the mean horizontal wind velocity provides a characteristic time which serves as a threshold for the computational time step. This time step should be smaller than the threshold since otherwise small patterns are not represented correctly along the trajectory path (Seibert, 1993). As typical mean wind velocities below altitudes of 20 km are smaller than 30 m s^{-1} (Malberg, 2006), the time step limit is as large as 73 sec by using the wind fields from the NWP model COSMO-2 with a horizontal resolution of 2200 m. Due to an extended length scale of the pattern in COSMO-7 and ECMWF, the time step could be even larger in these cases. With an internal temporal resolution of 15 sec employed in the match programme, truncation errors are expected to be negligible.
Interpolation errors arise from the necessity to estimate the wind field at locations in space and time between the grid points of a NWP model (Stohl *et al.*, 1995; Rolph and Draxler, 1990). The LAGRANTO scheme used for trajectory calculation solves this by linear interpolation in both cases as mentioned in Section 2.3.2. Stohl (1998) states that a linear interpolation in time is most accurate, but in space methods of higher order would improve the accuracy. Interpolation of the vertical wind component produces larger errors than interpolation of the horizontal wind due to its higher variability and missing routine

observations (Stohl and Seibert, 1998). Furthermore, small displacements in the vertical position of the air parcel would lead to large errors under conditions of significant wind shear (Kahl, 1996). This is supported by comparing calculated forward and backward trajectories. Whereas the quasi-horizontal trajectories of an air parcel vary only about a few hundred meters after travelled distances of a few hundred kilometres, balloon trajectories with a superimposed fixed climbing rate, differ up to one kilometre just after 30 min of transporting time. The effect of interpolation errors is generally dependant on the complexity of the weather situation. Weather situations with a strong height dependency of winds are problematic. Vertical geostrophic wind shear is a consequence of strong temperature advection and a baroclinic atmosphere, both a result of the thermal wind equation (Holton, 2004).
According to the literature (e.g. Pickering *et al.* (1996); Engström and Magnusson (2009); Stunder (1996)), very often wind field errors of the underlying NWP model are the largest error for trajectory calculations. Errors due to incorrect forecasts can be detected by comparing trajectories computed from forecast wind fields with those arising from analysis data, as it was done in the analysis of the match flight (Section 3.3.2). The observed RHTD of more than 20 % between the trajectories of COSMO-2 forecast and COSMO-2 analysis after 2 h travelling time agrees with Stohl (1998) who concludes: "Even for calculations that extend only shortly into the forecast period, average position errors of 30 % are typical." A few years later he compared the results from LAGRANTO with those from TRAJKS and FLEXTRA, two other trajectory models, and concludes following: "From an accuracy point of view the quality of the input data is more important than the choice among the three trajectory models" (Stohl *et al.*, 2001).
Note that most of the trajectory accuracy studies, Stohl (1998) included, deal with spatial and temporal resolutions of NWP models like ECMWF. An increase in both spatial and temporal resolution improves the accuracy of trajectories. Therefore a more precise trajectory calculation is expected for COSMO-2 and COSMO-7 inputs. Unfortunately no published study about COMSO-2 exists since the model became operational at MeteoSwiss in February 2008. The latest verification of COSMO-7, at that time referred to as Alpine Model, against profiler data of wind speed and wind direction is published by Arpagaus *et al.* (2006) based on data from the year 2004. However, this was done only up to 5 km altitude and for a forecast time of 12 h. Mean square errors near 3 m s^{-1} in wind speed and 20 $^\circ$ in wind direction were found as typical values. During our match flight on the 6$^{\text{th}}$ July lower errors in wind direction and speed occurred in this range of altitude and forecast time. Also the cumulative error after the first 120 min of the trajectory path at 6 km height stays smaller (Section 3.3.2).

In the context of the discussed trajectory errors the deviations between the simulated and recorded balloon flight paths are within usual ranges. After adjusting for the balloon's true ascent rate by using the vertical GPS information, the modelled balloon tracks matched also the horizontal GPS information reasonably well. For 6$^{\text{th}}$ July the observed trajec-

tory discrepancies between the forecast and the analysis of 20 % after 2 h travelling time is still in the range of common uncertainty. However, errors in the magnitude of even 10 % would imply a failing of the match. As defined in the project proposal the match radius is supposed to be smaller than 10 km (Peter and Spichtinger, 2008). An error of 10 % in relation to the distance travelled between Payerne and Zurich of approximately 135 km exceeds this limit. For the match flight performed and analysed the large wind field deviation between forecast and analysis does not affect the match accuracy in this extent as it did not occur in the target match level. Nevertheless a methodical investigation of deviations between trajectories calculated from forecast and analysis data over a longer period is required. As LAMMOC's focus on cirrus clouds is related to weather situations with large-scale flows – predicted usually with a high accuracy as a result of quite homogeneous wind patterns – it is essential to asses the role of the given weather situation. At the moment erroneous forecasts seem to be one of the biggest uncertainty and reason for potential match failure.

The aim of reaching a horizontal match radius better than 10 km was clearly achieved with the conducted match soundings. A vertical match radius is not specified, but with 1.4 km mean vertical extension of cirrus clouds (Dowling and Radke, 1990), the balloon could miss a cloud easily in the case of vertical displacement, if for example the rate of ascent of the balloon is incorrectly set. The vertical target level was clearly failed during the match in the second flight from Zurich. This problem is pointed out as the second major problem. A repetition has to be avoided in future by careful gas filling with the same preciseness as it is done in Payerne. Whether the aimed horizontal resolution of 10 km is chosen too large should be discussed after a couple of flights. Even widespread cirrus clouds with horizontal resolutions several times larger than the match radius might be difficult to analyse with respect to the cloud life cycle due to smaller patterns inside. The LIDAR provides this information and its use needs to be extended.

In summary, based on the experience of the flight on 6th July it seems to be possible to match an target air parcel with a radius much smaller than 10 km and additionally reach a match distance less than a few kilometres to air parcels below and above the target altitude level if the required vertical balloon velocity is met. Future match soundings will show whether the forecasting tool will perform successful as it seems to do after its first promising application.
The ongoing work and future prospects are outlined in Chapter 5. The task of trajectory modelling to forecast launching locations, times, and flight paths of match balloon soundings was performed within this diploma thesis. The transfer of the match technique to mid-latitude regions was technically a successful performance.

5 Outlook

A number of projects is likely to benefit from this thesis work in the near future. Some early measurements of the balloon-borne instruments are shown in Section 3.3.3, but are not analysed in detail. As this topic goes beyond the scope of this thesis, it will be covered by a bachelor project. The observed aerosol layer above the tropopause appears again in the backscatter profile of a single flight from Payerne about two weeks later at the end of July. It is weaker, but vertically more dispersed that time. Not only the LIDAR installed in Zurich, but also the LIDAR aboard CALIPSO observes this feature. A systematic assessment of the CALIPSO data of the last months and backward trajectory calculations for the time the aerosol layer was present might help to identify sources and footprints.
Another student's term paper carried out currently deals with an improvement of the balloon's rate of ascent. Aided by a physical parametrisation the fixed number of $5\,\mathrm{m\,s^{-1}}$ shall be replaced by a more realistic treatment of the balloon climbing. The balloon weight, the weight of the payload, the free lift, determined by the amount of used helium or hydrogen, and the contrary drag coefficient as a function of the atmosphere's density have to be considered for a more appropriate solution of the vertical velocity of rubber balloons (Yajima *et al.*, 2009). A complication is that the temperature of the balloon's lifting gas and the ambient temperature are not equal, as the inner temperature follows the outer temperature with a delay. A more precise simulation of the ascent could improve the match by a few kilometres and would be a useful correction of the existing programme version.

As this diploma thesis is embedded in the project of LAMMOC, the LAMMOC-funded doctoral thesis on that topic will make direct use this study. The tool developed will be applied at future forecasts for match soundings. Successful flights shall be analysed in more detail henceforth by running box models including microphysical cloud parametrisations. The processes of homogeneous and heterogeneous ice nucleation as well as growth, evaporation, and sedimentation of ice particles are included in a box model which can be coupled to trajectories calculated with LAGRANTO. Furthermore, an optical module in the box model shall calculate backscatter ratios with ice particle size distribution deduced from the modelled particles for comparison with COBALD data. Therefore, the backscatter coefficient of the particles at different wavelengths evaluated along the trajectories can be compared to those received by the match sonde.
Besides additional modelling work, the LIDAR installed recently on the roof of the institute's building can be applied. Three different modes of operation are foreseen. Vertically

pointing, the LIDAR observes the evolution above Zurich before, during, and after the balloon ascends. Alternatively, it can also scan along a predicted air parcel trajectory such that it points first upstream and later downwind of the sonde. The balloon's position, received real-time during the flight via GPS, could be included into the pointing algorithm of the LIDAR. By doing so a third option would be that the LIDAR tracks the balloon position ("shooting mode").
Finally, more frequent match soundings following by detailed analysis of the flight including modelling work and LIDAR results can be expected to provide a better appraisal of supersaturated regions inside cirrus clouds.

References

Arpagaus, M., Kaufmann, P., De Morsier, G., Ruffieux, D., Schubiger, F., Walser, A., and Zala, E. (2006). Verification of aLMo in the year 2005. *MeteoSwiss, COSMO Newsletter No. 6*. Available from `http://www.cosmo-model.org/content/model/documentation/newsLetters/newsLetter06/cnl6_arpagaus.pdf`.

Bud, R. (1997). *Instruments of science: An historical encyclopedia*. Routledge, 1 edition.

Consortium for Small-Scale Modelling (2009). COSMO LM model. Website. Available from `http://www.cosmo-model.org/`. Last accessed at 6th November 2009.

DeMott, P. J., Cziczo, D. J., Prenni, A. J., Murphy, D. M., Kreidenweis, S. M., Thomson, D. S., Borys, R., and Rogers, D. C. (2003). Measurements of the concentration and composition of nuclei for cirrus formation. *Proceedings of the National Academy of Sciences of the United States of America*, **100**(25), 14655–14660.

Dowling, D. R. and Radke, L. F. (1990). A summary of the physical properties of cirrus clouds. *Journal of Applied Meteorology*, **29**(9), 970–978.

Engström, A. and Magnusson, L. (2009). Estimating trajectory uncertainties due to flow dependent errors in the atmospheric analysis. *Atmospheric Chemistry and Physics Discussions*, **9**(4), 15747–15767.

European Centre for Medium-Range Weather Forecasts (2009). ECMWF model. Website. Available from `http://www.ecmwf.int/`. Last accessed at 6th November 2009.

Farman, J. C., Gardiner, B. G., and Shanklin, J. (1985). Large losses of total ozone in Antarctica reveal seasonal CLOx/NOx interaction. *Nature*, **315**(6016), 207–210.

Federal Office of Meteorology and Climatology MeteoSwiss (2009). COSMO LM model. Website. Available from `http://www.meteoschweiz.admin.ch/web/en/research/projects/cosmo.html`. Last accessed at 6th November 2009.

Finlayson-Pitts, B. and Pitts, J. (1999). *Chemistry of the upper and lower atmosphere*. Academic Press, 1 edition.

Fujiwara, M., Shiotani, M., Hasebe, F., Vömel, H., Oltmans, S. J., Ruppert, P. W., Horinouchi, T., and Tsuda, T. (2003). Performance of the meteolabor "Snow White" chilled-mirror hygrometer in the tropical troposphere: Comparisons with the Vaisala RS80 A/H-Humicap sensors. *Journal of Atmospheric and Oceanic Technology*, **20**(11), 1534–1542.

Fusina, F., Spichtinger, P., and Lohmann, U. (2007). Impact of ice supersaturated regions and thin cirrus on radiation in the midlatitudes. *Journal of Geophysical Research*, **112**(D24), D24S14–1–12.

Giannakaki, E., Balis, D. S., Amiridis, V., and Kazadzis, S. (2007). Optical and geometrical characteristics of cirrus clouds over a southern European lidar station. *Atmospheric Chemistry and Physics*, **7**(21), 5519–5530.

Heidemann, M. (2009). *Forecast for weather balloon flights*. Master's thesis, ETH Zurich.

Holton, J. R. (2004). *An introduction to dynamic meteorology*. Academic Press, 4 edition.

IPCC (2007). Climate Change 2007: The physical science basis. Contribution of working group I to the fourth assessment report of the Intergovernmental Panel on Climate Change [Solomon, S. and Qin, D. and Manning, M. and Chen, Z. and Marquis, M. and Averyt, K. B. and Tignor, M. and Miller, H. L. (eds.)]. *Cambridge University Press, Cambridge, United Kingdom and New York, NY, USA*, page 996.

Kahl, J. D. W. (1996). On the prediction of trajectory model error. *Atmospheric Environment*, **30**(17), 2945–2957.

Koop, T., Luo, B. P., Tsias, A., and Peter, T. (2000). Water activity as the determinant for homogeneous ice nucleation in aqueous solutions. *Nature*, **406**(6796), 611–614.

Labitzke, K. G. and van Loon, H. (1999). *The stratosphere: Phenomena, history, and relevance*. Springer, 1 edition.

Lorenc, A. C. (1986). Analysis methods for numerical weather prediction. *Quarterly Journal of the Royal Meteorological Society*, **112**(474), 1177–1194.

Lynch, D. K. (1996). Cirrus clouds: Their role in climate and global change. *Acta Astronautica*, **38**(11), 859–863.

Malberg, H. (2006). *Meteorologie und Klimatologie*. Springer, 5 edition.

Murphy, D. M. and Koop, T. (2005). Review of the vapour pressures of ice and supercooled water for atmospheric applications. *Quarterly Journal of the Royal Meteorological Society*, **131**(608, Part B), 1539–1565.

Nazaryan, H., McCormick, M. P., and Menzel, W. P. (2008). Global characterization of cirrus clouds using CALIPSO data. *Journal of Geophysical Research* , **113**(D16), D16211 (11 pp.).

Oolman, L. (2009). University of Wyoming. Upper Air Data: Soundings. Website. Available from `http://weather.uwyo.edu/upperair/sounding.html`. Last accessed at 6th November 2009.

Peter, T. and Spichtinger, P. (2008). Lagrangian measurements and modeling of cirrus clouds (LAMMOC). Research Plan.

Peter, T., Marcolli, C., Spichtinger, P., Corti, T., Baker, M. B., and Koop, T. (2006). When dry air is too humid. *Science*, **314**(5804), 1399–1402.

Petterssen, S. (1956). *Weather analysis and forecasting. Vol. I, Motion and motion systems*. McGraw-Hill.

Pickering, K. E., Thompson, A. M., McNamara, D. P., Schoeberl, M. R., Fuelberg, H. E., Loring, R. O., Watson, M. V., Fakhruzzaman, K., and Bachmeier, A. S. (1996). TRACE a trajectory intercomparison. 1. Effects of different input analyses. *Journal of Geophysical Research*, **101**(D19), 23909–23925.

Pielke, R. A. (2002). *Mesoscale meteorological modeling*. Academic Press.

Rex, M. (1993). *Stratosphärische Ozonabbauraten aus den Ozonsondendaten der EASOE-Kampagne*. Master's thesis, Georg-August-Universität Göttingen.

Rex, M. (1997). *Der Ozonabbau in der arktischen Stratosphäre: Ergebnisse einer neuen Messstrategie (Match)*. Ph.D. thesis, Freie Universität Berlin.

Rex, M., Harris, N. R. P., van der Gathen, P., Lehmann, R., Braathen, G. O., Reimer, E., Beck, A., Chipperfield, M. P., Alfier, R., Allaart, M., O'Connor, F., Dier, H., Dorokhov, V., Fast, H., Gil, M., Kyrö, E., Litynska, Z., Mikkelsen, I. S., Molyneux, M. G., Nakane, H., Notholt, J., Rummukainen, M., Viatte, P., and Wenger, J. (1997). Prolonged stratospheric ozone loss in the 1995–96 Arctic winter. *Nature*, **389**(6653), 835–838.

Rex, M., van der Gathen, P., Braathen, G. O., Harris, N. R. P., Reimer, E., Beck, A., Alfier, R., Krüger-Carstensen, R., Chipperfield, M., de Backer, H., Balis, D., O'Connor, F.,

Dier, H., Dorokhov, V., Fast, H., Gamma, A., Gil, M., Kyrö, E., Litynska, Z., Mikkelsen, S., Molyneux, M., Murphy, G., Reid, S. J., Rummukainen, M., and Zerefos, C. (1999). Chemical ozone loss in the Arctic winter 1994/95 as determined by the Match technique. *Journal of Atmospheric Chemistry*, **32**(1), 35–59.

Riddle, E. E., Voss, P. B., Stohl, A., Holcomb, D., Maczka, D., Washburn, K., and Talbot, R. W. (2006). Trajectory model validation using newly developed altitude-controlled balloons during the International Consortium for Atmospheric Research on Transport and Transformations 2004 campaign. *Journal of Geophysical Research*, **111**(D23), 1–13.

Rolph, G. D. and Draxler, R. R. (1990). Sensitivity of 3-dimensional trajectories to the spatial and temporal densities of the wind-field. *Journal of Applied Meteorology*, **29**(10), 1043–1054.

Rosen, J. M. and Kjome, N. T. (1991). Backscattersonde: a new instrument for atmospheric aerosol research. *Applied Optics*, **30**(12), 1552–1561.

Sassen, K., Wang, Z., and Liu, D. (2008). Global distribution of cirrus clouds from CloudSat/Cloud-Aerosol Lidar and Infrared Pathfinder Satellite Observations (CALIPSO) measurements. *Journal of Geophysical Research*, **113**(D8), D00A12 (12 pp.).

Schär, C., Leuenberger, D., Fuhrer, O., Lüthi, D., and Girard, C. (2002). A new terrain-following vertical coordinate formulation for atmospheric prediction models. *Monthly Weather Review*, **130**(10), 2459–2480.

Seibert, P. (1993). Convergence and accuracy of numerical methods for trajectory calculations. *Journal of Applied Meteorology*, **32**(3), 558–566.

Seinfeld, J. H. and Pandis, S. N. (2006). *Atmospheric chemistry and physics*. John Wiley & Sons, 2 edition.

Sprenger, M. (2006). Wettersysteme. Vorlesungsskript.

Steppeler, J., Doms, G., Schattler, U., Bitzer, H. W .and Gassmann, A., Damrath, U., and Gregoric, G. (2003). Meso-gamma scale forecasts using the nonhydrostatic model LM. *Meteorology and Atmospheric Physics*, **82**(1-4), 75–96.

Stohl, A. (1998). Computation, accuracy and applications of trajectories – A review and bibliography. *Atmospheric Environment*, **32**(6), 947–966.

Stohl, A. and Seibert, P. (1998). Accuracy of trajectories as determined from the conservation of meteorological tracers. *Quarterly Journal of the Royal Meteorological Society*, **124**(549, Part A), 1465–1484.

Stohl, A., Wotawa, G., Seibert, P., and Krompkolb, H. (1995). Interpolation errors in wind fields as a function of spatial and temporal resolution and their impact on different types of kinematic trajectories. *Journal of Applied Meteorology*, **34**(10), 2149–2165.

Stohl, A., Haimberger, L., Scheele, M. P., and Wernli, H. (2001). An intercomparison of results from three trajectory models. *Meteorological Applications*, **8**(2), 127–135.

Stunder, B. J. B. (1996). An assessment of the quality of forecast trajectories. *Journal of Applied Meteorology*, **35**(8), 1319–1331.

Vömel, H., Fujiwara, M., Shiotani, M., Hasebe, F., Oltmans, S. J., and Barnes, J. (2003). The behavior of the Snow White chilled-mirror hygrometer in extremely dry conditions. *Journal of Atmospheric and Oceanic Technology*, **20**(11), 1560–1567.

von der Gathen, P., Rex, M., Harris, N. R. P., Lucic, D., Knudsen, B. M., Braathen, G. O., Debacker, H., Fabian, R., Fast, H., Gil, M., Kyrö, E., Mikkelsen, I. S., Rummukainen, M., Stähelin, J., and Varotsos, C. (1995). Observational evidence for chemical ozone depletion over the Arctic in winter 1991–92. *Nature*, **375**(6527), 131–134.

Walmsley, J. L. and Mailhot, J. (1983). On the numerical accuracy of trajectory models for long-range transport of atmospheric pollutants. *Atmosphere-Ocean*, **21**(1), 14–39.

Warren, S. G., Eastman, R. M., and Hahn, C. J. (2007). A survey of changes in cloud cover and cloud types over land from surface observations, 1971-96. *Journal of Climate*, **20**(4), 717–738.

Wernli, H. and Davies, H. C. (1997). A Lagrangian-based analysis of extratropical cyclones. I: The method and some applications. *Quarterly Journal of the Royal Meteorological Society*, **123**(538, Part B), 467–489.

Yajima, N., Izutsu, N., Imamura, T., and Abe, T. (2009). *Scientific ballooning*. Springer, 1 edition.

Acknowledgements

This master thesis was written at the Institute of Atmospheric and Climate Science at ETH Zurich as part of my Landscape Ecology studies at the University of Münster. The stay abroad was temporarily financed by the German Academic Exchange Service (D/09/40739).

Besides all people, who were involved in this project, I would like to thank in particular...

Prof. Dr. Thomas Peter, der es mir ermöglicht hat, meine Diplomarbeit in seiner Arbeitsgruppe zu schreiben. Sein großes Interesse an meiner Arbeit hat mich sehr motiviert. Darüber hinaus danke ich ihm für die Unterstützung bei der Teilnahme am SCOUT und WaVaCS Workshop in Schliersee, sowie für die Einladung zum Gruppenseminar in Lichtenstein.

Prof. Dr. Otto Klemm für seine Bereitschaft, mir auch während der Zeit meiner externen Diplomarbeit ständig als Ansprechpartner zur Verfügung zu stehen. Über den Rahmen der Diplomarbeit hinaus möchte ich ihm herzlich für die Zeit als studentische Hilfkraft in seiner Arbeitsgruppe danken.

Dr. Frank Wienhold für die Unterstützung und Geduld, die er mir von Anfang an entgegen gebracht hat, für die vielen Gespräche, die hilfreichen Tipps, für die Betreuung und das Gegenlesen meiner Arbeit. Ich freue mich auf die zukünftige gemeinsame Zusammenarbeit.

Martin Brabec for his assistance with COBALD and Ana Cirisan for interesting discussions and joint learning. Both supported the match flight in Zurich together with Tanja Dallafior.

Gonzague Romanens, Gilbert Levrat, and the team of MeteoSwiss in Payerne for their attendance and support during the match flight.

Dr. Michael Sprenger, Dr. Urs Beyerle und Dr. Daniel Lüthi für die Bereitstellung der COSMO- und ECMWF-Daten und die Lösung vieler technischer Probleme. Michael Sprenger möchte ich speziell dafür danken, dass er Teile meiner Arbeit so hilfreich kommentiert hat.

Dr. Johanna Gietl, Jennifer Sobiech und Roland Wittler für das sorgfältige Korrekturlesen dieser Arbeit.

Torsten Tritscher, der mir während der gesamten Dauer meiner Diplomarbeit zur Seite stand. Er hat nicht nur die Arbeit durch gute Ideen und Korrekturvorschläge verbessert, sondern mir auch die nötige Ruhe zum Schreiben gegeben. Danke für alles.

Meinen Eltern Agnes und Johannes Engel, die mir das Studium durch ihre großzügige Finanzierung ermöglicht und all meine Entscheidungen stets unterstützt haben.

Statement

I assure, that I did this entire thesis myself including figures, tables, and maps, if not mentioned differently, and did not use any other aid than specified in the text. Text, literal or analogous, originating from other sources is marked with its original source.

Zurich, 12th November 2009 .....

Ines Engel